Revised file Clean version - For Typesetting Click here to view linked References

Challenges and Strategies for Imidazolium Ionic Liquids as Novel Phase Change Materials for Low and Medium Temperature Thermal Energy Storage: A Critical Review

Qi Li [a], Chunyun Yang [a], Shaohui Wang[a], Meimei Zhou[a], Huicheng Xie [a], Geng Qiao [b], Yanping Du [c], Chuan Li [a,*], Yuting Wu [a]

[a] MOE Key Laboratory of Enhanced Heat Transfer and Energy Conservation, Beijing Key Laboratory of Heat Transfer and Energy Conversion, Beijing University of Technology, Beijing, 100124, China
[b] Global Energy Interconnection Research Institute Europe GmbH, 10117 Berlin, Germany
[c] School of Engineering, Lancaster University, Lancaster LA1 4YW, UK
Corresponding author: lichuan@bjut.edu.cn

Abstract

This review aims to provide an insight into the imidazolium ionic liquids (ILs) as novel phase change materials (PCMs) for low and medium temperature thermal energy storage, with a focus on their multi-dimensional thermophysical/nucleation features within encapsulation for defect regulation during solid-liquid transition. Imidazolium ILs have been emerging as novel phase transition-based energy storage material due to unique properties of wide liquidous range, rich crystallization behavior, small thermal volumetric expansion and environmental-friendly properties, but suffer from defects of low enthalpy and large supercooling. To meet the challenge acting as PCMs, the work first gave a brief overview on supercooling regulation and enthalpy elevation of imidazolium ILs, and proposed micro-encapsulation with crystallization-promoting porous shell to regulate their defects. Then discussion regarding multi-dimensional thermophysical features of imidazolium ILs were given, including features within micro-confined capsule core (phase transition, melting point, thermal stability, specific heat capacity and thermal conductivity), nano-confined nucleation within the mesoporous shell, and mesoporous interfacial nucleation. Finally, the future applications of imidazolium ILs and microencapsulation in the fields of infrared stealthy, solar thermal utilization, thermal management in extreme environment and green energy-saving building were highlighted. The study provides a timely review of the imidazolium ILs acting as thermal energy storage (TES) materials, and future suggestion like functional ILs with more hydrogen bonds or supercooling utilization for seasonal TES may help concentrate efforts on solving the key issues in urgent

need.

Keywords: Imidazolium Ionic Liquids; Phase Change Materials; Supercooling; Thermal Energy Storage; Phase Transition Behavior

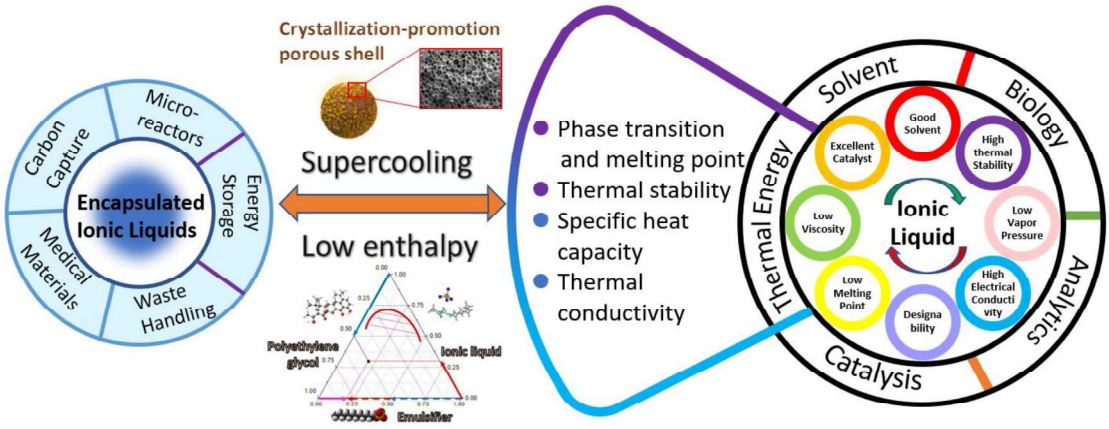

Thermophysical features of imidazolium ionic liquids and their defects regulations (supercooling and low enthalpy) as phase change materials are comprehensively reviewed.

1. Introduction

During the past decades, energy storage have been attracting dramatically growing attention as CO_2 reduction technologies, attributed to the fact that it allows excess energy to be stored and transferred back to its original or different form when needed, including forms of electrochemical, mechanical, thermal and electrical[1, 2]. Among these options, thermal energy storage (TES) is a promising and safe option as it stores energy in the form of heat, cold or a combination of both in a storage material. TES can be further classified into sensible heat storage (SHS), latent heat storage (LHS) and thermochemical energy storage (TCHS) based on the type of heat. LHS using PCMs is particularly appealing attributed to the high energy storage capacity, quasi-isothermal charging/discharging process, and reasonable capital investment. As a functional and smart material, PCMs can be classified based on their phase state (solid-liquid, solid-solid, solid-gas, or liquid-gas), chemical composition (organic, inorganic, eutectic mixture), and melting temperature range (low, mid, or high temperature). This makes PCMs

widely used in various applications such as solar or wind energy systems, building, refrigeration, textiles.

Within the scope of TES, the low temperature often refers to the range of -100 ~ 250 ℃ (shown in Fig.1a). For example, logistics of COVID-19 vaccines require storage temperature of -80 ~ -60 ℃ (BioNTech) and -25 ~ -15 ℃ (Moderna and Janssen)[3], refrigeration space demands PCMs functionalize at temperatures of -40 ~ 28 ℃[4], temperature control of vehicle cabin at -50 ~ 70 ℃ and battery protection at 30 ~ 80 ℃[5, 6], thermal protection of electronic device at 25 ~ 50 ℃[7], food thermal protection at -30 ~ 120 ℃[8], and solar thermal energy storage at temperatures of 20 ~ 150 ℃[9]. As given in Fig.1b, organic compounds (paraffins, fatty acids, polyalcohols) and inorganic salt hydrates are the most investigated PCMs for low temperature TES. Organic PCMs have high melting enthalpy and undergo minimal volume change during phase transition, but they have low thermal conductivity. Salt hydrates, on the other hand, have higher thermal conductivity and cost effective but are not compatible with metallic containers and suffer from phase separation. Eutectic mixtures of inorganic salts may experience congruent transition without stratification, but they still face challenges such as supercooling tendency and poor cycling stability. Previous studies have extensively reviewed the thermophysical properties or challenges of low temperature PCMs[10-14]. So far, it is safety to say no individual PCMs can perfectly meet all requirements in the field of thermal energy storage. Consequently, there is an increasing demand for new energy materials that offer ideal thermal properties while also being safe, cost-effective, and stable for specific applications.

The inorganic molten salts, which are typically mixtures of alkali salts such as carbonate, nitrate, fluoride or chloride, have gained popularity in today's energy technology at medium and high temperature range of 200 ~ 1000 ℃, attributed to their high latent heat and low costs. Ionic liquids (ILs), on the other hand, are a special group of molten salts that consist of large organic cation and a small inorganic anion. They normally have lower melting temperature compared to inorganic salts due to their larger molecular volumes and internal competition between Van der Waals and Coulombic forces. By selecting appropriate anions/cations, functional groups or alkyl chains, their thermal properties can be optimized within a wide range of -96 ℃ ~ 359 ℃[15]. There are vast number of potential combinations of cations and anions, estimated to be around

one billion, which provides a significant scope for tailoring ILs to specific application[16, 17]. Over 1000 ILs have already been synthesized, surpassing the number of conventional inorganic salts available[18]. Due to properties of stable thermal/chemical, adjustable polarity, wide liquid and electrochemical window, ILs have been widely used as reaction media for various green chemical process or as electrolytes[19]. However, less frequent is their application in thermal energy storage as PCMs because the advantage of applying those media are not that straightforward.

Among the vast choice of ILs, imidazolium cationic-based ILs have been studied extensively to realize tunable physicochemical properties. The electronic structure of classic imidazolium cation ring is best described as comprising two nitrogen atoms interconnected by methylene group, which categorized as N1 (amoino nitrogen) donor and N3 (imino nitrogen) acceptor as given in Fig.1c. Tunable properties of imidazole can be achieved as second amine can participate into varies amphoteric reactions. Classic low-temperature ILs anions include bis(trifluoromethylsulfonyl)imide (NTf_2^-), trifluoromethylsulfate (TfO^-), dicyanamide ($N(CN)_2^-$), tetrafluoroborate (BF_4^-), hexafluorophosphate (PF_6^-), and anions not in liquid state at room temperature including chloride, bromide, iodide, nitrate, perchlorate, formate or acetate. For ILs serving as PCMs, published data of their thermophysical properties and enthalpy is still limited, but the interaction role influencing thermal properties is clear: hydrogen bonding, ion size, charge dispersity, alkyl branching and ion symmetry[20]. Table 1 compared the energy storage indexes of imidazolium ILs and commercial energy storage materials. Obviously, the sensible storage density and thermal conductivity of ILs are higher than these of commercial media respectively, while the latent energy storage density is relatively lower. Nevertheless, the overall storage density of imidazolium ILs is competitive with commercial ones, thus have been used in the field of solar power energy storage[21].

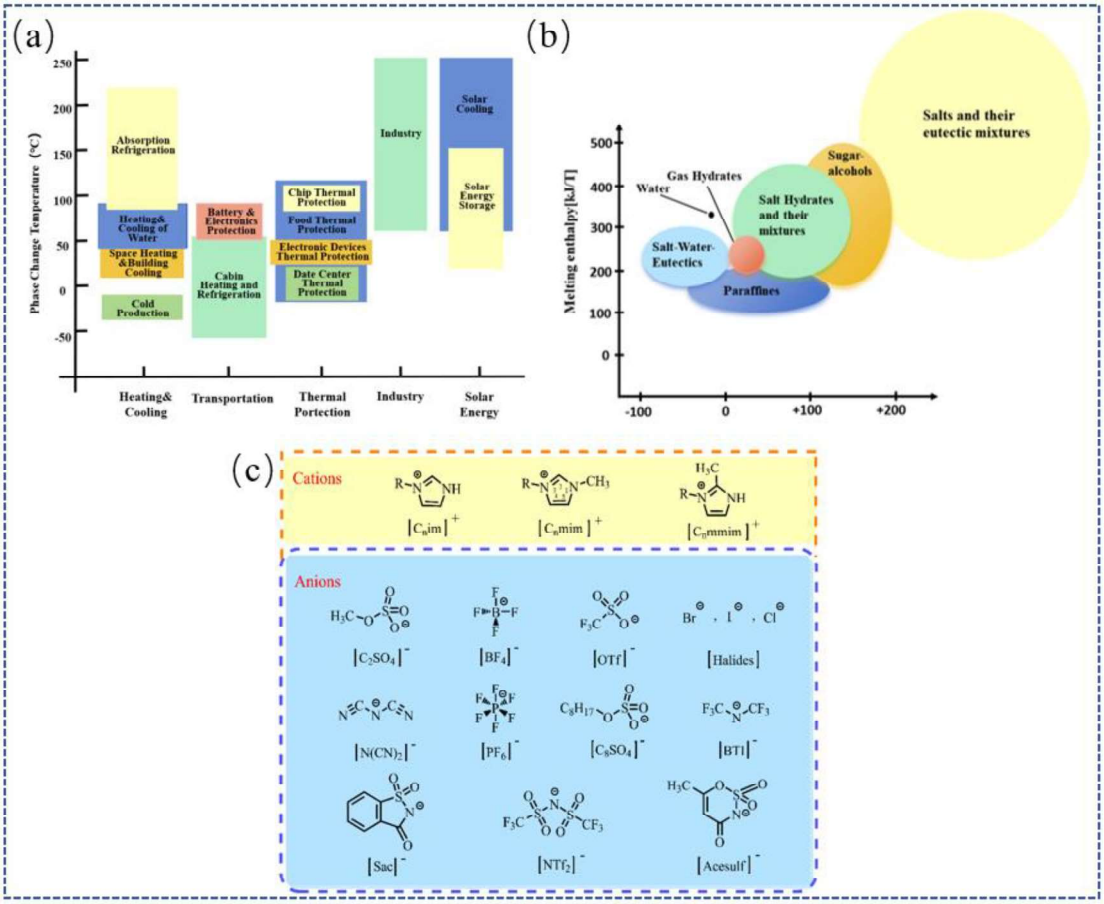

Fig.1. (a) Low temperature PCMs a) applications of PCMs at temperature range of -50 ~ 250 ℃[12], (b) PCMs in the temperature range of -100 ~ 200 ℃ against melting enthalpy[22]; (c) Chemical structures of the main cations and anions used in imidazolium ILs.

Table 1 Energy storage indexes of imidazolium-based ILs and commercial energy storage medium

	Energy storage medium	ρ ($g \cdot cm^{-3}$)	T_m (℃)	T_d (℃)	C_p ($J \cdot g^{-1} \cdot K^{-1}$)	ΔH_f ($J \cdot g^{-1}$)	$\Delta E_{sensible}$ ($MJ \cdot m^{-3}$)	ΔE_{latent} ($MJ \cdot m^{-3}$)	P_V (kPa)	λ ($W \cdot m^{-1} K^{-1}$)	μ (Pa·s)
ILs	$[C_2MIM][BF_4]$[21]	1.25	14.42	445.49	1.28	48.2	160.9	60.4	<< 101.32	0.200	36.07
	$[C_2MIMM][BF_4]$[21]	1.17	87.38	423.73	1.66	-	194.9	-	<< 101.32	0.18	119.78
	$[C_2MIM][NTf_2]$ [23, 24]	1.4	-15	280	1.2	52.96	180	74.14	<< 101.32	0.12	268.8
Commercial energy storage medium	VP-1[21]	1.06	12	400	1.78	97.3	144.7	-	85.11	0.13	24.8
	Tetradecane[25, 26]	0.76	10.6	122	2.07	225.6	-	174.24	0.13	0.14	1.57

***Advantages of imidazolium ionic liquids as PCM*:** The rich crystallization behavior, small volumetric expansion as well as environmental-friendly properties make imidazolium ILs potential candidate for phase transition-based energy storage materials[27], especially at the low temperature range. Table 2 gives the thermophysical properties of the main imidazolium ILs from recent literatures. Imidazolium ILs exhibits heat of fusion of 59.00 ~ 159.00 kJ/kg upon melting range of – 87 ℃ ~ 208 ℃. The high heat of fusion can be found at long-chain alkylimidazolium halogen ([C_{16}MIM]Br or [$C_{16}C_1$IM]Cl) with melting range around 64.00 ℃. Their decomposition temperature (T_d), however, are normally lower than that with $[NTf_2]^-$ or $[TfO]^-$ anions. The highest and lowest T_d can be found at [C_3MMIMI][Im] (423.85 K) and [$C_2H_3O_2$BIM]Br (201.85 K). The heat capacity and thermal conductivity of imidazolium ILs falls in the range of 0.17 ~ 1.82 (J/g·K) and 0.125 ~ 0.186 ($W \cdot m^{-1}K^{-1}$), respectively.

Table 2. Thermophysical parameters of the main imidazolium ILs acting as PCMs

Ionic Liquids	T_m (℃)	ΔH_f (J/g)	T_d (℃)	C_p (J/g·K)	λ ($W \cdot m^{-1}K^{-1}$)	Ref
[C_2MIM][NTf_2]	-14.90	55.20	-	1.34	0.128 ~ 0.130	[23, 28, 29]
[C_2MIM][BF_4]	14.85	48.19	444.85	1.28	0.200	[23, 29, 30]
[C_2MIM][PF_6]	-	70.24	-	-	-	[23]
[C_2(MIM)$_2$][BF_4]$_2$	144.82	94.41	355.94	-	-	[31]
[C_2(MIM)$_2$](Br)$_2$	188.32	116.26	310.66	0.87 (100 ℃)	-	[32, 33]
[C_2(MIM)$_2$][NTf_2]$_2$	139.63	73.99	452.41	-	-	[31]
[C_2(MIM)$_2$][PF_6]$_2$	191.34	109.41	388.73	-	-	[31]
[C_2(MMIM)$_2$](Br)$_2$	110.12	17.86	248.40	-	-	[32]
[$C_2H_3O_2$BIM]Br	156.85	46.37	201.85	-	-	[34]
[$C_2H_3O_2$MMIM]Br	147.85	57.92	304.85	3.77	-	[34]
[$C_2H_3O_2$MIM]Br	176.85	104.21	291.85	1.81	-	[34]
[C_2H_5OMIM]Br	71.85	78.04	303.85	1.72	-	[34]
[C_2(eim)$_2$](Br)$_2$	184.21	125.17	305.19	0.83 (100 ℃)	-	[32, 33]
[C_2(pim)$_2$](Br)$_2$	102.88	60.15	298.94	-	-	[32]
[C_2(bim)$_2$](Br)$_2$	99.93	54.42	280.39	-	-	[32]
[C_3(MIM)$_2$](Br)$_2$	172.80	115.82	321.24	-	-	[31]
[C_3MMIMI][Im]	10.80	97.30	456.85	1.20	0.131	[21, 35]
[C_4(MIM)$_2$](Br)$_2$	115.45	155.69	318.33	0.87(100 ℃)	-	[32, 33]

$[C_4MIM][MeSO_4]$	-	-	320.85	-	0.172 ~ 0.179	[36]
$[C_4MIM][BF_4]$	-87.38	-	423.85	1.62~1.66	0.159 ~ 0.186	[21, 37, 38]
$[C_4MIM][BF_6]$	10.85	-	-	1.45	0.136~0.173	[37, 39-41]
$[C_4(eim)_2](Br)_2$	131.34	102.13	277.33	0.94 (100 ℃)	-	[32]
$[C_4MMIM]Cl$	92.89	76.38	-	-	-	[42]
$[C_4MIM]Cl$	74.00±1.00	18.00±0.50 (kJ/mol)	-	-	-	[30, 43]
$[C_4MIM]Br$	-	74.39	214.85	-	-	[23, 29]
$[C_4MIM][NTf_2]$	-6.31	53.49	330.00	-	0.124 ~ 0.128	[44]
$[C_4MMIM]Br$	76.51	66.98	-	-	-	[23]
$[C_4(MMIM)_2](Br)_2$	32.45	86.70	330.59	-	-	[32]
$[C_4H_6O_2MMIM]Br$	149.85	92.95	237.85	2.32	-	[34]
$[C_4H_6O_2BIM]Br$	92.85	45.53	208.85	2.06	-	[34]
$[C_4(C_2H_4im)_2](Br)_2$	116.01 ~ 134.86	159.35	304.36	0.81 (100 ℃)	-	[32, 45]
$[C_4(C_2H_5Oim)_2](Br)_2$	102.92 ~ 103.07	110.20	297.65	1.41 (100 ℃)	0.125 ~ 0.127	[32, 45]
$[C_4(C_2H_3O_2im)_2](Br)_2$	208.62	117.85	309.43	-	-	[32]
$[C_6MIM][NTf_2]$	-	63.2	-	-	0.125 ~ 0.127	[23, 28]
$[C_6MIM][BF_4]$	-	-	357.85 ~ 440.85	1.445 ~ 2.284	0.158 ~ 0.167	[46-48]
$[C_8MIM][BF_4]$	11.55	20.06 (kJ/mol)	404.00	1.63		[24, 49]
$[C_8MIM][Tf_2N]$	-	-	400.00	1.23	0.125 ~ 0.128	[49]
$[C_8MIM][PF_6]$	-	-	405.00	1.59	-	[49]
$[C_{10}MIM]Br$	74.43	66.79	-	-	-	[23]
$[C_{10}MMIM]Br$	68.20	75.39	-	-	-	[23]
$[C_{16}MIM]Br$	63.91	152.56	-	1.25 ~ 1.79	-	[23]
$[C_{16}MMIM]Br$	98.55	126.62	-	1.27 ~ 3.09	-	[23]
$[C_{16}C_1IM]Cl$	64.00	159.00				[50]

1

In terms of cold chain storage, temperature is not the single parameter affecting the deterioration rate and postharvest lifetime of food, extrinsic factors such as humidity and CO_2 concentration also matter. For example, the standard of air-conditioned cold storage is required to be adjustable within the range of – 2 ~ 15 °C, relative humidity RH of 75 ~ 95%, and CO_2 content of 1 ~ 10%. PCMs with anti-virus and antibacterial functions will be favorable due to the appearance of global epidemic. Imidazolium ILs can be employed as PCMs in cold chain logistics because 1) Imidazolium ILs have powerful adsorption and desorption capacity of CO_2 both physically and chemically[51] (16 % less energy requirement and 11% reduction than the aqueous amine), leading to an increased gas regulatory space in cold chain storage without secondary pollution; 2) Imidazolium ILs have superior water sorption (reaching 0.5 g/g at 20 ℃/70% RH) and fast sorption rate under wide humidity range [52], leading to a wide adjustable humidity range; 3) Imidazolium ILs have shown remarkable improvement in the activity of ciprofloxacin[53]. The antibacterial properties can be further improved with the addition of metal ions to imidazole-based coordination, which will be of great importance in cold chain environment during the global epidemic; 4) Thin film induced by the chemical reaction of imidazolium ILs and steel surface can prevent container corrosion, while traditional PCMs like organic and hydrate salts are usually corrosion when in direct contact with metal housings or pipes. In a word, the crucial features of adjustable melting temperature range, antibacterial, anti-corrosion, and adjustable humidity and gas composition promote imidazolium ILs perfect multi-functional energy storage medium for cold chain logistics.

Another benefit of imidazolium IL is their high stability under radioactive environment, which is favorable in thermal control of spacecraft under extreme environment from direct solar irradiance to near total darkness. Rao et al.[54] examined various imidazolium ILs γ-irradiated to absorbed dose levels up tp 700 kGy, and found little changes in density, viscosity and refractive index in spite of the significant variation in color and electrochemical window. Similarly, it has been proven that radiation have a negligible effect on the interfacial properties and phase behavior of imidazolium IL-based microemulsions with different alkyl chain lengths[55]. Inspired by the unique property, NASA (National Aeronautics and Space Administration, USA) launched project of ‘Modified Ionic Liquids-Based Phase Change

Materials as Effective Heat Exchangers' during 2016 – 2019[56] (shown in Fig. 2a). The developed PCM formulations exhibit high enthalpy (254 - 272 kJ/kg) upon low volume expansion (~ 6 - 7%), as well as high thermal diffusivity, thermal inertia, without corrode metallic substrates, phase separation or degrade. Therefore, imidazolium-ILs can be developed as the next-generation PCMs given their various advantages.

Until now, many efforts have been made to review ionic liquid & ionanofluids as thermal fluid[35, 57-59], but very limited consolidated study focused on ionic liquids' rule as phase change materials. A recent review from Piper et al.[20] showed ionic liquids offer a series of inherent "green" properties that translate well into the field of phase change materials, and emphasized the importance of computational methods to tailor the thermal properties of ILs. Matuszek et al.[60] studied the potential of protic ionic liquid as phase change materials, and the results showed small structural variations in the cation may lead to a drastic changes in thermophysical properties in the intermediate temperature range. They also recommend ILs functionate to mitigate the intermittency issue of wind and solar energy in intermediate temperature range (100 ~ 220 ℃)[61]. Urzúa et al.[62] compared the thermal storage density of ionic liquid mixtures, and found the value surpasses that of some conventional materials utilized for energy storage. While data of ILs' properties like density or viscosity are sufficient, reports on ILs' phase transition properties (e.g. ΔH_f, ΔS_f) is very few. Besides, a systematic review on imidazolium ILs' supercooling and transition characteristics is still lacked despite of their rich crystallization behavior and high stability. To the best of authors knowledge, no work or published data were given to meet the challenge of imidazolium ILs for thermal energy, such as regulating supercooling, elevating heat enthalpy or reducing phase separating. In contrast, research with regard to tunable and green ILs as PCMs showed a prosperous upward tendency in the past 12 years (shown in Fig.2b). To meet the challenge of ionic liquids working as PCMs, this review attempts to find a solution to reduce ILs' effective viscosity, avoid solid-liquid transition leakage, decrease phase separation and supercooling simultaneously firstly, by overviewing methods of supercooling regulation and enthalpy elevation of imidazolium ILs. Then it summarizes thermophysical properties of imidazolium ILs within the encapsulation core, phase transition of nanoconfined ILs inside the capsule shell, as well as nucleation characteristic on

porous surface. Finally, the future applications of imidazolium ILs and microencapsulation in various industrial fields are discussed.

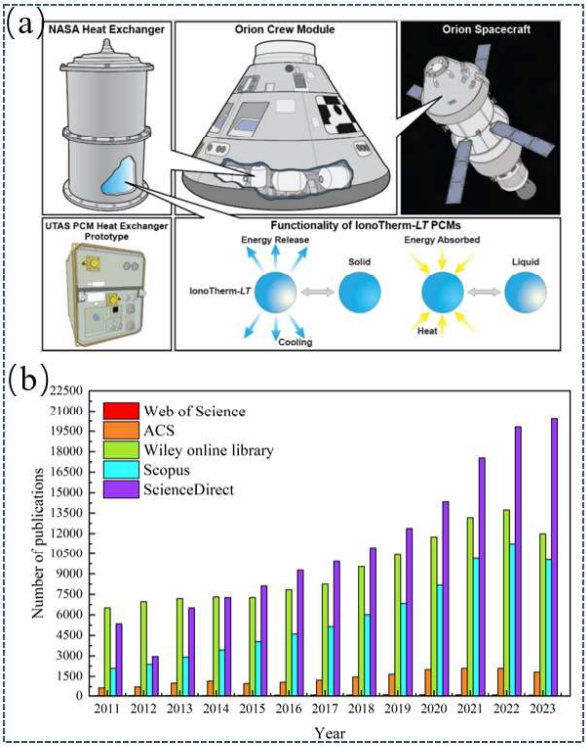

Fig.2. (a) Modified Ionic liquid-based PCMs utilized in effective heat exchanger in extreme space environment from NASA[56].Number of publications that include 'ionic liquids as phase change materials' in the title, abstract or keywords during the past 12 years (data obtained from ScienceDirect, ACS, Wiley, Web of Science and Scopus in Oct 2023)

2. Challenge and strategies for ionic liquids as phase change materials

2.1 Supercooling regulation

Despite the vast advantages of ILs as PCMs, the low enthalpy of pure solution and supercooling are still the main concern defects[63, 64]. Supercooling is a metastable state generated during materials' solid-liquid transition, providing energy for crystal growth and crystal plane expansion, also known as the driving force of phase change crystallization. Supercooling and glass formation are processes typical for ILs with imidazolium cations, and in extreme cases crystallization maybe kinetically restrained. Although thermophysical optimization by anion selection or by changing the chain-length of aliphatic non-polar domains is feasible, the complicated synthesis process and expensive plant-scale progress hindered its potential

development. To implement ILs into PCM-based application, technologies to conquer the defects should be proposed. The main methods to regulate ILs' supercooling can be divided into the following two categories.

1). *Introducing heterogeneous nucleation point to reduce nucleation barrier*. Many efforts have been made to increase nucleation points by adding nanoparticles[65], surfactants[66], etc. The addition of such materials can simultaneously improve the thermal conductivity and induce interfacial rotational crystallization. The crystal form, concentration, morphology and size of additives determines the nucleation and crystallization performance, while improper addition may inhibit crystallization and improve the supercooling[67, 68]. With the development of energy storage, a single nucleating agent can no longer meet the requirements for the regulation of the supercooling of PCMs. Yet a systematic understanding of the action mechanism of composite nucleating agents is still lacked[67].

Adding nanoparticle addictive to host have been proven to be the simplest yet most effective way to promote heterogenous nucleation, because crystallization can be notably modified when moderate interactions presents[69]. Although adding nanoparticles to ILs[57, 70] to elevate thermal conductivity has been widely studied, their effects on ILs nucleation were scarcely investigated. Efimova et al.[43] employed microcrystalline powders of SiO_2, AlN, $CaCO_3$ and MgO (1 ~ 3 wt%) as nucleating seeds, but the crystallization kinetics of [C_4MIM]Br was nearly unaffected. They also tested the homogeneous nucleation agent – 1 ~ 3 wt% [C_4MIM]Cl, but no thermal effects present. In a recent study, carbon nanotubes (CNTs) was added to 1-[4′-(4″-nitrophenylazo)-phenyloxy] hexyl-3-methyl-1H-imidazol-3-ium tetrafluoroborate to test their impact on crystallization process[71]. The results revealed the fusion enthalpies of the composition crystals were 29.3 ~ 32.2 kJ/mol and the crystallization enthalpy increased by 20%, due to the increased crystal nucleation rate caused by the π-π interactions between the molecule and the rigid CNT surface. Similar suppressing effect can also be achieved by adding graphite, hexagonal boron nitride and graphene oxide.

Encapsulation in the confined space of microcapsules or hollow fibers can solve the problem of solid-liquid phase change leakage, reduces phase separation and improves the efficient

thermal conductivity. For liquid-solid PCMs in a confined space, the main nucleation mechanism transfers from heterogeneous nucleation in bulk system to homogeneous nucleation in encapsulated counterpart, due to the dramatically increased amount of surface alkane molecules (also known as surface freezing monolayer). Confined space favors the development of surface freezing, meaning the temperature range of two rotator phases expanded. A study of n-docosane crystallization behavior showed a new metastable rotator phase emerge alongside with the surface freezing [72]. In terms of binary mixtures in microcapsules, the solid-solid phase separation was inhabited due to suppressed interactions of the terminal methyl-methyl in the confined spaces, resulting in higher miscibility of the two components.

2). *Stimulating nucleation sites by physical field intervene*. The commonly used ways using external field to promote heterogeneous nucleation are ultrasonic vibration, electric field and magnetic field. Cavitation caused by ultrasonic vibration continuously break the crystals. The broken crystals will fuse with melted solution, leading to an improved dispersion of crystal nucleus and providing sufficient nucleation sites for heterogeneous nucleation[65]. The intervention of electromagnetic field can accurately control the grain size by change the chemical potential difference and charge distribution. When applying electric field on molecular solution, the induced dipole emerged due to the increased charge separation between polar and non-polar molecules. The induced dipole interacts with the electric field, which changes the free energy of the molecule and the polarization orientation of the molecular chain, and affects the stacking arrangement and crystal morphology of the molecular chain[73] (as shown in Fig.3). Magnetic field can significantly reduce the supercooling time of polymetallic materials, but its effect on nonmetallic PCMs is still controversial[74].

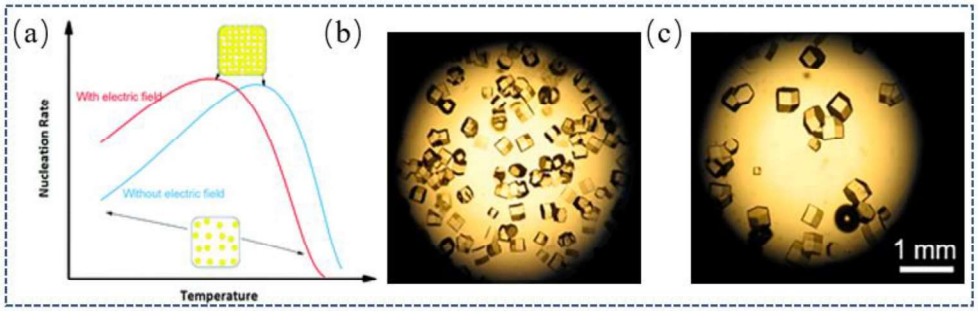

Fig.3. (a) Schematic diagram of the effect of electric field on nucleation rate and phase transition temperature[75]; (b) and (c) is the optical microscope images of HEWL crystal in

sodium chloride solution under no electric field and 2.36V/cm electric field, respectively, indicating the electric field increases the crystal size but decreases the number of crystals[73].

Other schemes to reduce supercooling include using metal foam or nanowires to disturb the crystallization of phase change materials[76], regulating the surface tension to drive the crystal trend at the liquid-liquid interface[77], and so on. Many of these schemes cannot simultaneously solve the problems of supercooling, phase separation and leakage, and sometimes lose the inherent advantages of phase change materials, which is not practical in industrial applications. Therefore, confining composite materials in a micro-space to suppress supercooling/phase separation and elevate enthalpy simultaneously is one of the most promising methods to regulate ILs' defects.

2.2 Enthalpy elevation

Low enthalpy is another defect hindered imidazolium ILs' application as PCMs, even though new emerged ones have shown improved enthalpy of fusion. Many efforts have been devoted to increase ΔH_f by enhancing electrostatic and hydrogen bonding interaction among cationic and anionic ions[33, 45], by means of elongating length of alkyl linker chain, or substituting functional groups or cationic moieties[78]. However, the synthesis process is rather complicated and ΔH_f is still relatively low (159 kJ/kg for $[C_4(C_2H_3IM)_2]Br_2$[45]) compared with conventional PCMs (271.9 kJ/kg for C_{15} - C_{18} alkanes[79]). Nevertheless, the enthalpy of ILs can be elevated by adding polar or non-polar compounds with higher enthalpy, as IL possesses power of diversity and versatility in solvent-being polar and non-polar (alphatic chains in the cations) simultaneously [80].

Among the conventional PCMs, polyethylene glycol (PEG) was a common semi-crystalline polymer with high enthalpy (~ 185.6 J/g [81]) and often utilized to form form-stable composite PCMs at low temperature range. Tunable physicochemical properties can be obtained by changing PEG chain lengths, and the thermal conductivity of organic PEG can be enhanced by 63.0 ~ 87.7 % with the addition of nano-materials (graphene oxide [82] or AgNWs [83]). Blending ILs with PEGs are also known as 'hybrid green' systems with fascinating properties of non-volatility, good polarity, low flammability and excellent miscibility strength[84]. Special

attention should be paid to the solubility and phase behavior, as they determined the overall thermophysical features of homogeneous solvents, biphasic system, or immiscible solution with possible phase separation.

Due to the high hydrogen bond acidity of imidazolium cation, stronger hydrogen bonds can be reached when PEG acting as a proton acceptor. Visak and co-workers[85, 86] revealed the phase behavior of imidazolium ILs-PEG solution for various ILs' cation/anion, as well as PEG or alkyl chain lengths[86]. Imidazolium IL and PEG200/ PEG400 are mutually miscible, attributed to the intermolecular interactions of PEG and ILs caused by hydrogen bonding and ion-dipole interactions[87]. The effect of anions on solubility of $[C_2mim]^+$-based ILs and solid PEG2050 follows the order of $[EtSO_4]^-$ < $[OTf]^-$ <$[NTf_2]^-$, attributed to the interplay between ILs' cation-anion, anion-PEG and PEG-PEG. Therefore, one can mix highly hydrophilic PEG with hydrophobic bistriflamide ILs or hydrophilic ILs with longer cation alkyl chain, to form homogeneous solution or as liquid biphasic system.

The imidazolium chloride ILs may also form immiscible liquid mixtures with PEG of large molecular weight. Total miscible have been found for PEG1000 in $[C_2mim]Cl$, as well as PEG1000 and PEG1500 in $[C_4mim]Cl$[88], attributed to stronger Coulombic forces of $[C_2mim]Cl$ than the longer alkyl chain (shielding effect). The mole fraction of IL in the PEG-rich phase (0.83 ~ 0.99) was significantly higher than PEG in the IL-rich phase (0.02 ~ 0.38) over the temperature range of 60 ~ 140 ℃. Similarly, an density functional theory (DFT) analysis revealed that the interaction energy between $[C_nMIM]Br$ and PEG decreased with increasing length of the alkyl chain of ILs[89]. A super-viscosity was found in the mixtures of $[C_4MIM][BF_4]$ with PEG400 and PEG1000, meaning viscosity of mixture was significantly higher than that of single pure component[90]. The viscosity of the alkyl imidazolium-based ILs with PEG200 follows the order of $[C_4MIM][BF_6]$ > $[C_4MIM][BF_4]$ > $[C_2MIM][BF_4]$, because the cation size of $[C_2MIM]^+$ is not large enough to facilitate the interactions. To evaluate the viscosity of binary mixtures, the McAllister model[91] was used as:

$$\ln\eta = x_1^3 \ln\eta_1 + x_2^3 \ln\eta_2 + 3x_1^2 x_2 \ln\eta_{12} + 3x_1 x_2^2 \ln\eta_{21} - \ln\left(x_1 + x_2\frac{M_2}{M_1}\right) + 3x_1^2 x_2 \ln\left(\frac{2 + M_2/M_1}{3}\right) + 3x_1 x_2^2 \ln\left(\frac{1 + 2M_2/M_1}{3}\right) + x_2^3 \ln\frac{M_2}{M_1} \quad (1)$$

where η_{12} and η_{21} is the interaction parameters respectively, M_i and η_i refers to molecular mass and viscosity of pure component i, respectively.

Conclusively, the super-viscosity phenomena of PEG-ILs hybrid solution hampered the widespread implementation in advanced applications. Confining the hybrid solution inside microcapsule with crystallization-promoting shells can effectively suppress supercooling, decrease phase separation, reduce efficient viscosity and prevent solid-liquid transition leakage.

3. Simultaneous strategy for defect regulation: encapsulation ionic liquids (ENILs)

Confined IL morphologies had widespread applications in CO_2 recovery, microreactors, and heavy metal removal [92]. The most feasible IL capsulation method included sol-gel, emulsion interfacial polymerization, or loading hollow capsules (shown in Fig.4). Other fabrication methods include chemical sedimentation, solvent evaporation, and spraying suspension dispersion[83, 93, 94]. Weiss et al.[95] prepared Pd/[C_4MIM][PF_6]@SiO_2 encapsulation using sol-gel method for the application of heterogenized catalyst. A high content (> 85% w/w) of [C_4MIM][$FeCl_4$] in hollow porous carbon sub-microcapsules was fabricated for the purpose of NH_3 gas capture[96]. In the field of electrochemical capacitors, Pentzer and co-workers[97] encapsulated ionic liquids using Pickering emulsions and graphene oxide nanosheets as sole surfactant. A summary of ENILs and according thermophysical parameters were listed in Table 3. An obvious conclusion drawn is that the study of ENILs in the field of thermal energy storage just started exploring.

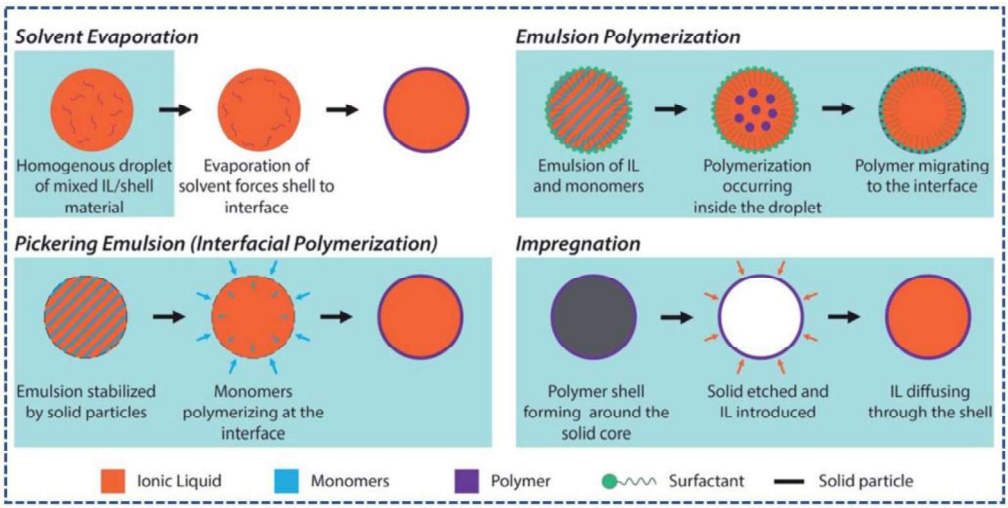

Fig.4. Schematic representations of different methods used for fabrications of encapsulated ionic liquids[98].

Table 3. Thermophysical properties of imidazolium ENILs. Rows are color to indicate four main types of shell materials including Polyurea, Silica, Polysulfone and Polymers.

Shell material	Encapsulation method	Ionic liquid	IL loading ratio (wt%)	Particle size (μm)	Thermophysical features	Surface morphology		Application scenario	Ref
						Micropore volume (cm^3/g)	BET surface area (m^2/g)		
Polyurea	Emulsion polymerization	$[C_4MIM][PF_6]$	20	2 ~ 80 (average: 22)	T_d = 287 ℃	-	-	Catalyst, separation, energy	[99]
Polyurea	Interfacial polymerization	$[C_4MIM][PF_6]$	46 ~ 71	27 ~ 105 (wall thickness ~ 3.8)	T_d = 300 ~ 410 ℃	-	-	Lubricant	[100]
GO (Graphene Oxide)-Polyurea	Interfacial polymerization	$[C_4MIM][PF_6]$	65 ~ 80	50 ~ 125	T_g = -70 ℃, T_m = -20 ℃, T_d = 250 ℃	-	-	CO_2 capture	[101]
GO-Polyurea	Pickering emulsion	$[C_2MIM][2\text{-}CNpyr]$	50 ~ 60	40 ~ 50 (wall thickness ~ 4)	T_d = 200 ~ 360 ℃	-	-	CO_2 capture	[102]
GO-Polyurea	Pickering emulsion	$[C_2MIM][TFSI]$ $[C_2MIM][DMP]$ $[C_4MIM][BF_4]$ $[C_4MIM][PF_6]$ $[C_6MIM][TFSI]$ $[C_4M_2IM][PF_6]$	55 ~ 83	10 ~ 35; 30 ~ 60	T_d = 200 ~ 500 ℃	0.000176 ~ 0.000501	0.104 ~ 0.203	Phenol Extraction	[97]
rGO (Reduced Graphene	Interfacial polymerization	$[C_4MIM][PF_6]$	77 ~ 78	25 ~ 100 (wall thickness of 10 ~ 15)	T_d = 200℃, T_m = 11 ℃,	0.007180 ~ 0.160500	0.250 ~ 90.790	Electrochemical capacitors	[92]

Oxide)-polyurea									
Alkylated GO-Polyurea	Pickering emulsion	$[C_2MIM][TFSI]$ $[C_6MIM][TFSI]$	78 ~80	10 ~ 50; 5 ~ 25	NA	0.006223 ~ 0.006342	74.550 ~ 75.370	CO_2 capture	[103]
Polyurethane	Interfacial polymerization -Pickering emulsion	$[C_4MIM][PF_6]$	20	<20	T_d = 200 ~550 ℃	-	-	-	[104]
SiO_2-Polyurethane	Sol-gel	$[C_4MIM][PF_6]$	31	2 ~ 14	T_d = 120 ℃	-	-	-	[105]
SiO_2	Sol-gel	$[C_4MIM][PF_6]$	50 ~ 70	1 ~ 10	T_d = 200 ~ 500 ℃	0.017000 ~ 0.045000	36.000	CO_2 capture	[106]
	Sol-gel	$[C_4MIM][PF_6]$	60 ~ 70	4 ~ 7	T_d = 200 ~ 400 ℃	-	-	CO_2 capture	[107]
	Interfacial polycondensation	Pd/$[C_4MIM][PF_6]$	66	Average size of 3.6	T_d = 185 ~ 650 ℃	-	47.400	Heterogenization of catalysts	[95]
	Interfacial polymerization	$[C_4MIM][PF_6]$	35	1~5	T_d = 384℃	-	-	Knoevenagel condensation	[104]
Polysulfone	Chemical precipitation	$[C_4MIM][PF_6]$	50 ~ 70	1 ~ 10	T_d = 200 ~ 500 ℃	0.019000 ~ 0.047000	41.000	CO_2 capture	[106]
	Solvent evaporation	$[C_2MIM][NTf_2]$	53	Average size of 128 (wall thickness of ~10)	T_d = 440 ℃ T_g = 110℃	-	-	In situ self-lubricating composites	[94]

	Solvent evaporation	$[C_2MIM][Tf_2N]$	37	0.7~3	T_g = 146.03 ℃, T_m = -17.75 ℃, T_c = -44.65 ℃	-	-	CO_2 capture	[108]
	Solvent evaporation	$[C_4MIM][Tf_2N]$	43	0.6~5	T_g = 130.75 ℃, T_m = -3.14℃, T_c = -17.01 ℃	-	-	CO_2 capture	[108]
	Solvent evaporation	$[C_6MIM][Tf_2N]$	47	0.8~5.5	T_g = 118.37 ℃	-	-	CO_2 capture	[108]
	Solvent evaporation	$[C_4MIM][Tf_2N]$ +Fe_2O_3/CuO/TiO_2	27~ 49	Average size of 1	T_d = 323 ~ 464 ℃; T_g = 137 ℃, T_m = -3.4 ℃; T_c = -24.7 ℃	-	-	CO_2 capture	[109]
	Phase inversion	$[C_4MIM][PF_6]$	32	Average size of 44.2	T_d = 500.81 ℃	-	-	Wastewater Treatment	[110]
	Spraying suspension dispersion	$[C_4MIM][PF_6]$	29	Average size of 70	T_d =356.27℃	-	-	Catalysis, separation	[93]
	Solvent evaporation	$[C_6MIM][PF_6]$	26	Average size of 5	T_d =514℃	-	-	Lubricant	[111]
Polystyrene	Suspension polymerization	$[C_4MIM][PF_6]$	61	Average size of 388	T_d = 200 ~400 ℃	-	-	CO_2 capture	[107]
Polystyrene	Interfacial polymerization	$[C_2MIM][PF_6]$	80±1	8~40, Average size of 23	Tm = 89.7 ℃, ΔH_f = 139.7 J/g, Tc = 76.9 ℃	-	-	Thermal energy management	[112]

								and carbon capture	
Poly(thiourethane) and poly(amide-thioether)	Interfacial polymerization	$[C_2MIM][TFSI]$ $[C_6MIM][TFSI]$	70	100~250, 60~200 (wall thickness of 10~15)	T_d = 286 ℃ T_d = 287℃	-	-	-	[113]
Poly(methyl methacrylate)	Interfacial polymerization	$[C_2MIM][PF_6]$	76±10	Average size of 21	-	-	-	Thermal energy management	[112]
Polyethylene	Interfacial polymerization	$[C_2MIM][PF_6]$	72±9	Average size of 22	-	-	-	Thermal energy management	[112]

3.1 Thermophysical behavior of imidazolium Ionic Liquids

The US National Institute of Standards and Technology (NIST) collects most accessible literature references regarding thermophysical properties of ILs[23], but phase transition characteristics of imidazolium ILs and dependences of thermodynamic properties on IL structure are not fully explored. Therefore, enriching the related information is pivotal to further development of imidazolium IL-based PCMs for latent heat thermal energy storage applications.

3.1.1 Phase transition and melting point

Exact determination of IL melting point is difficult because the salts show tendency to supercooling and formation of glass[63]. Strong supercooling has been frequently reported for ILs, especially under conditions of high cooling/heating rates or short time scales. Thus, IL's crystallization may not be detected by common DSC device due to nucleation suppression. Regardless of ILs' physical states (liquid, amorphous, or polymorphous crystalline), the main influencing factors of their supercooling is intrinsic properties (conformational equilibria, solid polymorphism, high viscosities, etc.) and experimental factors (cooling rates, time scale)[64]. Different crystals are phases with different conformational composition instead of distinguishable phases[114], caused by the competition between pairwise long-range repulsion and short-range attraction[115].

The imidazolium ILs may undergo multi-stage phase transition, which varies with different cation/anion structures, heating/cooling rate or annealing treatment conditions. As shown in Fig.5a[116], the nanocrystal domains of $[C_{10}mim][NO_3]$ were independently appear at the first stage, followed by orientational correlation among the nanocrystal dominated the second period, which was essential to form crystal domain on a mesoscopic scale. At the last stage, a long-range homogenous layer structure appeared, and crystal growth process cannot continue due to the apparence of a partial pinning effect caused by nano-heterogeneity and weak ionic between cations and anions. The cation or anion structure could significantly influence these multi-step transition process. For example, $[C_2MIM][TFSI]$[117] underwent solid-solid transition at 230 K, where crystal phase had a long periodic layered structure; and inhomogeneous melting transition at 257 K, where the lattice constant along the stacking direction showed no similarity

with the correlation length in the solid state[116].

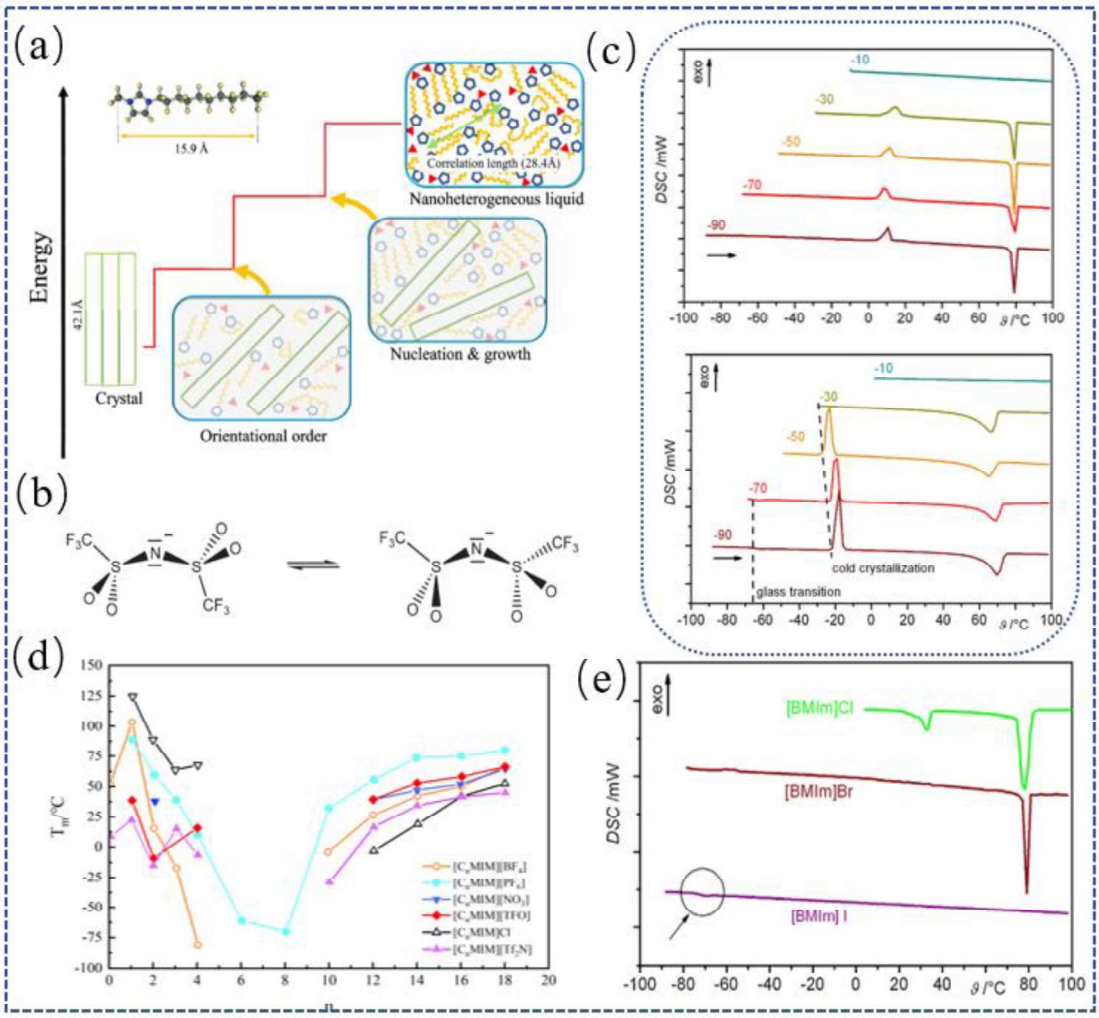

Fig.5. (a) Multistep phase transition processes upon cooling[116]; (b) Conformational equilibrium of $[Tf_2N]^-$ ion with the two CF3 groups trans- and cis- to one another[118]; (c) DSC measurements of the thermal behavior of $[C_4MIM]Br$ without and with annealing step at T_{min} [43]; (d) $[C_nMIM]$-based ILs' melting point versus the alky chain length for $[C_nMIM][BF_4]$, $[C_nMIM][PF_6]$, $[C_nMIM][NO_3]$, $[C_nMIM][TFO]$, $[C_nMIM]Cl$ and $[C_nMIM][Tf_2N]$[119]; (e) Melting behavior of $[C_4MIM]X$ (X = Cl, Br, I) [43]

The rotational or orientational disorder in ILs' crystal state, also known as an internal rearrangement of molecule(s) around one or more axes, will lead to the appearance of solid-solid phase transition. The glass or plastic behavior tend to lower ILs' fusion enthalpy and decrease their advantage properties as PCM. As shown in Fig.5b, $[Tf_2N]^-$ exhibits two forms of conformational equilibria (trans- and cis- conformers), attributed to different steric and electronic environments. Varies equilibria features will lead to different thermophysical

properties, which rationalized their low melting points and low viscosity[118]. To understand the crystal polymorphs and phase transitions, the crystal energy landscape was proposed as the distribution of protentional energy minima in a crystal structure, which was influenced by the conformational flexibility of the crystal[120]. Rotnicki et al.[117] found [C_2MIM][TFSI] formed a crystal monoclinic structure where molecular group move rotationally at T = 10 K ~ 230 K. Similarly, crystallography analysis of [PyH][CH_3SO_3] suggested that glass crystal were caused by dynamic change in cation or anionic -CH_3/-CF_3 group[60]. To quantitively evaluate the glass crystal, the thermodynamic magnitudes embroiled during phase transition can be rationalized in terms of 'beads', $\Delta C_p(T_g)/R$, described as movable units corresponding to molecules and their degrees of freedom. Similarly, the fragility index m, derived from empirical correlations[121-123] at transition stage, can be used to characterize the glass-forming liquid:

$$\mathrm{m} = 56\frac{T_g}{\Delta H_m}\Delta C_p \tag{2}$$

$$\mathrm{m} = 34.7\frac{T_m}{\Delta H_m};\ \Delta C_p \equiv 34.7\frac{\Delta C_p}{\Delta S_m} \tag{3}$$

$$\mathrm{D} = \frac{(T_g/T_K)-1}{0.0255};\ S_c(T) = \Delta_{fus}S - \int_T^{T_{fus}} \frac{C_p(glass)-C_p(crystal)}{T}dT \tag{4}$$

Where ΔH_m , T_K, D, S_c(T) is the enthalpy of melting, Kauzmann temperature, fragility parameter, and supercooling parameter respectively. Small value of fragility index (i.e. D = 7.4 for [C_6MIM][Tf_2N]) usually represents a fragile liquid.

The phase transition characteristics of IL are significantly influenced by the cation/anion combination, heating/cooling rates and annealing condition[50]. Due to the slow kinetics of ILs' phase transition, high cooling rates normally induces stronger supercooling or incomplete crystallization. For example, the rotational motions of [C_{10}MIM][NO_3]'s alkyl chains were randomly frozen at high cooling rate (> 9 ℃/min), thus their crystal nucleation and phase transition were suppressed. At low melting rate (5 – 8 ℃/min), a multistep phase transition induced by the serious motions of the alkyl chains were generated. Similarly, [C_4MIM][NO_3] exhibited multistep phase transition upon slow cooling (< 2.0 ℃/min), but crystallization was not induced above 3.0 ℃/min[116]. [$C_{16}C_1$IM]Cl showed a stable triclinic crystalline phase on slow cooling of 1 ℃/min, while fast quenching (12-13 ℃/min) from a temperature below the

isotropization temperature may lead to a mixture of triclinic phase and unstable perpendicular double bilayer[50]. Triolo et al.[64] found low cooling rate (≤ 0.02 K/s) introduced crystallization of [C_4MIM][PF_6], while high cooling rates lead to the amorphous solid or glass below glass-transition temperature (T_g = 194 K, T_m = 284 K). The ratio of T_g/ T_m = 0.68 or $T_g \approx (2/3)T_m$ was typically an indication for good glassy formation[123], defined as a nonequilibrium state of material where certain degrees of freedom of molecular motion were frozen in. It was noteworthy that the first heating scan of DSC should not be used, because the heat transfer equilibrium between the sample and measurement cell material was not readily established[50].

Annealing parameters (such as temperature, rate and duration) can significantly affect materials microstructure during the crystallization process, which is very common in alloy processing. By introducing an "annealing" step - keeping temperature constant for a period of time, ILs' solidification behavior significantly distinguished from the sample without annealing. As given in Fig.5c, [C_4MIM]Br only exhibited high-viscosity glassy state when cooling down to -30 ~ -90 ℃, while the annealing step introduces cold crystallization when cooling down to -50 ~ -90 ℃. Paulechka et al.[124] found [C_2MIM][NTf_2] crIV was formed if the sample was kept at 236 ~ 252 K before calorimetry measurements, while crI was formed at the annealing temperature of < 235 K or > 260 K. Triolo et al.[64] detected a second crystallization transition upon isothermal treatment of the supercooled liquid [C_4MIM][PF_6]. The annealing step can influence the conformational flexibility of both the cations and anions in ILs. When heating or cooling ILs with anions containing a N-S bond, the annealing process can lead to internal rotation around the bond or in the alkyl chain. By promoting internal rotation, the annealing step can change ILs' conformation and ultimately influencing their properties.

Besides cooling rate and annealing step, the cation/anion structure also has a strong connection with phase transition behavior for vast types of ILs. Increasing ions size, anisotropy or internal flexibility will lower ILs' melting temperature, while increasing dispersive interactions among alkyl chains will increase their melting temperature. In terms of imidazolium ILs, torsional motion in the alkyl chains will lead to coexistence of multiple conformers[118], and affects ILs' molecular packing, intermolecular interactions or distance, and ultimately their properties. As

given in Fig.5d, melting points of $[C_nMIM]^+$ displayed a remarkable decreasing tendency with the growth of chain length for short alkyl chain ($C_n < 6$) due to better ion cohesion, and increase with the alkyl length ($C_n > 8$) caused by the hydrophobic cations and large Van der Walls interaction[125]. The inflection point, however, varies depends on the anion type. For nitrate salts, supercooling of $[C_2MIM][NO_3]$ reaches 53.3 ℃, while no crystallization was observed for ILs with longer chain ($C_n > 4$). Thus, the crossover alkyl chain length ILs ($C_n = 4$) can be treated as an intermediated state between the crystal ($C_n = 2$) and glass states ($C_n = 6 \sim 8$), and a glassy was superimposed in to the crystal state at low cooling rate. The phenomenon indicates the nano-heterogeneity was well developed and thus could affect the crystal nucleation and growth at low temperature. For imidazolium ILs with $[NTf_2]^-$ anions, the glass transition temperature of $[C_4MIM][NTf_2]$ and $[C_6MIM][NTf_2]$ is 181.5 K and 184.3 K, respectively, obtained by heating the glass liquid above their de-vitrification temperature[114]. In the case of homologous imidazolium salts with $[PF_4]^-$ as anion, the length of alkyl chains has a significant impact on phase behavior and properties. For cations with short alkyl chains ($C_n \leq 3$), the compounds tend to exhibit crystalline phases with relatively high T_m due to densed packing of the molecules[118]. With the increase of alkyl chains ($4 \leq C_n < 12$), the behavior of ILs shifts towards a wider liquidus range with lower T_m (-81.1 ~ 26.5 ℃), as well as prominent tendency of supercooling. When the alkyl chains become longer ($C_n \geq 12$), complex phases can emerge with liquid-crystalline characteristic, where the molecules have a certain degree of orientational order while retaining fluid-like behavior.

Many attempts were made to analyze the role of anion in ILs' melting, while the effect is still blur and the electron pattern and hydrogen bond formation capability seems to be the main factors. Interaction energy calculation of $[C_4MIM]X$ showing the energy, as well as melting temperature decreases with the anion order of $[SCN]^- < I^- < [NO_3]^- < Br^- < Cl^- < F^-$. As shown in Fig.5e, $[C_4MIM]Cl$ exhibits enantiotropic polymorphism with phase transition and melting at 30 ℃ and 74 ℃[43], respectively. $[C_4MIM]Br$ melts at 78 ℃ and the recrystallization fails with a glassy solid formed, and $[C_4MIM]I$ experience solidification without crystallization, with amorphous substance arise at -70 ℃. The difference of phase transition temperature is attributed to the anion size. The overall lattice energy of $[C_4MIM]Cl$ is higher than that of $[C_4MIM]I$ due

to larger ionic radius of iodide anion. For $[C_2MIM]^+$ alkyl salt with sulfate anion, ILs show an increasing tendency of melting point with the growth of anion alkyl chain length[125]. However, given the enormous numbers of cations/anions combination, the potential collections of ILs are quite staggering and fetching their melting point experimentally at low consumption seems impossible. As a powerful and reliable tool, the machine learning methods were developed based on corelating physicochemical features with the existence data. Venkatraman et al.[15] predicted the melting points of structurally diverse 2212 ionic liquids with 1369 cations and 141 anions using quantitative structure-property relationship-based (QSPR) methods, which is more accurate for ILs with melting point above and below 100 ℃. Keshavarz et al.[126] proposed a T_m correlation based on atoms in cationic and anions structures as well as correcting functions of specific cation/anion moieties, which has been proven to be reliable and feasible in a wide range of different ILs types. Generally, the machine learning method can yield relatively accurate melting point of ILs, which is a promising tool for ILs' screening and synthesis.

3.1.2 Thermal stability

Near the decomposition temperature, IL's anion will attack pairwise cation, resulting in the cleavage of C-N bond contained S_N2 and S_N1 pathways[127]. Thus, the mechanism of ILs' degradation process has been proven to be the substituent reaction. Plenty of work have been published on the decomposition mechanisms[56, 128, 129], where pseudo-zero-order rate expression or empirical formula (Kissinger, Ozawa-Flynm-Wall, Coats-Redfern) can be used to describe the thermal decomposition kinetics, and no further discussion will be given here.

Although thermo-gravimetric analysis coupled with mass spectrometry (TGA-MS) is the most widely measurement method, it can hardly reveal the real decomposition temperature of ILs because 1) reported temperature based on TGA measurements vary based upon the sample mass, sample pan material, atmosphere type and flow rate[130, 131], while these influence parameters not always reported making comparisons to literature values difficult. Meanwhile, the water content, volatile impurities and evaporation of ILs also contributed to the mass loss[132]. Given the fact that chemical change after heating pure ILs can be detected by absorption spectroscopy, the total synchronous fluorescence spectroscopy was employed to explore ILs' decomposition

sensitively. As given in Fig.6a, the fluorescence spectra of $[C_8MIM][Tf_2N]$ exhibited new peaks at longer wavelengths after heating, attributed to the decomposition of $[C_8MIM]^+$ into two chromophore products 1-octylimidazole and 1-methylimidazole. The decomposition temperatures from fluorescence method was found to be 140 ℃ lower than the TGA measurement. Similarly, Del Sesto et al.[133] found significant changes in color and concomitant in the UV-Vis spectra of $[C_4mpy][Tf_2N]$ when heating above temperature of 150 ℃, where no detectable mass loss was captured using TGA. Therefore, extra care must be taken when drying ILs to avoid the formation of fluorescence impurities. 2) Previous study have shown the decomposition temperature of imidazolium and pyrrolidinium ILs were significantly lower than T_{onset} [133]. To evaluate long-term stability, the temperature at which the decomposition of ILs researches 1% for a given time ($T_{0.01/x}$) was suggested[134]. Using this definition, the decomposition temperature of $[C_4mpy][Tf_2N]$ was found to be 271 ℃, while T_{onset} were reported to be near 400 ℃[133] from TGA. Cao and Mu[135] compared the D-value between T_{onset} and $T_{0.01/10h}$ upon 60 ILs, and found a moderate linear relationship dependence of cation-anion combination.

The cation-anion combination (alkyl chain length, substituent position, anion type and IL family), heating rate, atmosphere and experimental conditions can significantly influence their thermal stabilities. Judging by T_{onset}, the ILs' thermal stabilities vary from least stable (T_{onset} < 250 ℃) to most stable (T_{onset} > 450 ℃) by altering the anion and cation. Generally, shorter alkyl chain length causes lower Van der Waals forces, leading to an increased intramolecular electrostatic interaction and higher thermal stability[136], but the overall impact of ILs' chain length on thermal stability is minimal. In the case of imidazolium ILs with the same cation ($[C_4MIM]^+$), the thermal stability increases with decreasing hydrophilicity in an anion order of $[Ac]^-$ < Cl^- < Br^- < $[NO_3]^-$ < $[TFO]^-$ < $[BF_4]^-$ < $[Tf_2N]^-$ < $[PF_6]^-$. Halide anions clearly reduced the decomposition temperature, i.e. the 1-butyl-3-methylimidazolium halide ILs are stable only up to 238 ~ 260 ℃[43]. $[C_6MIM]^+$ exhibited higher thermal stability when paired with $[Tf_2N]^-$ rather than $[BF_4]^-$ or $[PF_6]^-$ anions[132], and the thermal stability of $[C_8MIM]^+$ is also higher with $[Tf_2N]^-$ anion due to the weaker nucleophile. Therefore, ionic liquids with $[Tf_2N]^-$ anion showing low viscosity and high thermal stability are now preferred[118].

Thermal ramp rate not only influenced ILs' crystal features, but also significantly changed the thermal degradation temperatures. Usually, slow heating results in lower decomposition temperature for DSC scans. As shown in Fig.6b, the decomposition temperature of [C_8MIM][TfO] and [C_8MIM][Tf_2N] decreased by ~ 23 K and ~13 K respectively when heating rate lowered from 10 to 2 ℃/min[137], because lower heating rate allowed for the ILs' temperature to equilibrate and exhibited less thermal lag. For imidazolium ILs, the thermal decomposition of anion usually occurred several degrees before cation decomposition. Similar conclusion was drawn for various types of IL by many researchers[128, 138-140].

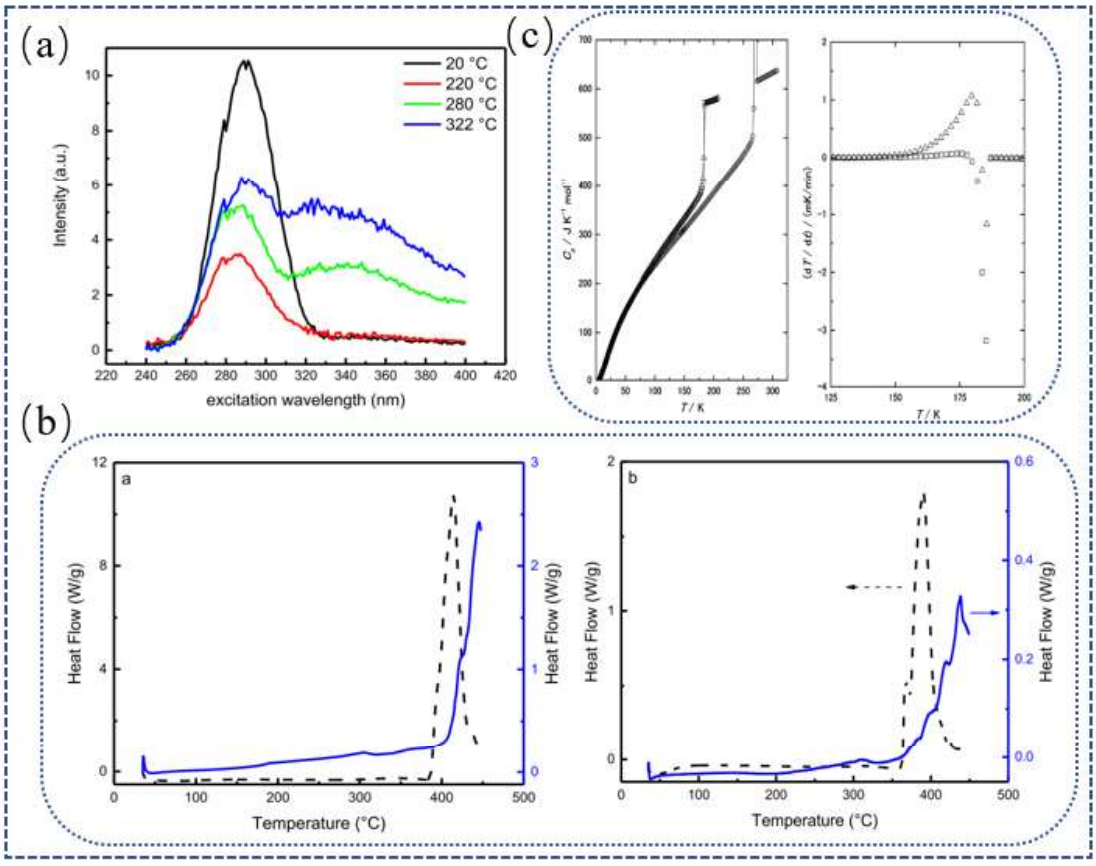

Fig.6. (a) Synchronous fluorescence spectra of diluted [C_8MIM][Tf_2N] using a wavelength interval of 50 nm[137]; (b) DSC measurement of [C_8MIM][Tf_2N] (Blue solid line) and [C_8MIM][TfO] (black dash line) from 35 to 450 ℃at a heating rate of 10 ℃/min and 2 ℃/min[137]; (c) Heat capacities of liquid and solid states of [C_6MIM][Tf_2N] and temperature drifts around a glass transition[123].

3.1.3 Specific heat capacity

The heat capacity of ILs was significantly influenced by the alkyl length, anion type, hydrogen bond network, as well as working temperature [76, 141, 142]. Compared to the vast amount of simulation work, the experimental information of ILs heat capacities is relatively scarce. For most ILs with clear phase change transition, anomalies in heat capacities occur due to the formation of metastable crystals. The metastable condition was caused by a certain degree of conformational or orientational disorder of anion, as the phenomenon was observed for all compounds of $[C_nMIM][NTf_2]$ but not in $[C_nMIM]Br$. A correlation equation for heat capacity calculation of liquid $[C_nMIM][NTf_2]$ was proposed by Paulechka et al.[124]:

$$C_{p,m} = (b_0 + b_1 n) + 10^{-2}(c_0 + c_1 n)T + 10^{-4}(d_0 + d_1 n)T^2 \quad (5)$$

where b, c and d are the parameters obtained from experimental heat capacities under various temperatures. The heat capacities of liquid imidazolium ILs changes almost linearly with temperature (T = 258 K ~ 370 K) at constant pressure to volume[143]. However, when measuring the solid ILs, careful treatment should be taken as usual DSC procedure may result in incomplete crystallization condition named liquid-quenched glass (LQG). To obtain c_p of solid $[C_6MIM][Tf_2N]$[123], the sample was held around 215 K for a few days before exothermic started, and the exothermic process may last three days (shown in Fig.6c). The heat capacity of LQG was slighter larger than the stable crystal ones, suggesting the molecular packing in LQG was looser than that of the crystal. As a result, the heat capacities of imidazolium ILs are not only sensitive to the thermal history, but also the phase transition and consequently of the measurement setup geometry on the measured values[144].

3.1.4 Thermal conductivity

For molecular solvents like simple linear alcohols, the thermal conductivity was expected to increase with decreasing molecular size of compounds[145]. However, the dependence of imidazolium ILs' thermal conductivity on cation and anion type was not so straightforward. Their thermal conductivity kept decreasing with alkyl lengths up to 6 carbons[28], due to ILs' nanostructures and the phonon-hopping effect[146]. Then the value increased with alkyl chain lengths from 6 to 10 carbons, which can be rationalized by higher energy barrier induced by larger apolar domains with increasing alkyl length, as well as the reduction of highly conductive

polar domain triggered by the 'Dilution effect'[147]. In terms of anions, it is found the thermal conductivity of $[C_4N_3]^-$ and $[BF_4]^-$ anions were significantly higher than that of $[FAP]^-$ and $[Tf_2N]^-$ [57]. Oster et al[145]. found the anions of $[P_{14,6,6,6}]$-based ILs has little influence on their thermal conductivity, or the differences fell in the in the standard uncertainty of the measurement. However, establishing a straightforward relationship between the ions size and resulting thermal conductivity is difficult due to the complex nature of intermolecular interactions.

As given in Table.2, the thermal conductivity of imidazolium ILs settles around the range of 0.113 ~ 0.238 W/(m·K). Some ILs (>0.170 W/(m·K)) have higher thermal conductivity than traditional fatty acid PCMs, such as octoic acid, decanoic acid, myristic acid etc. Castro et al.[148] found $[C_nMIM][PF_6]$ exhibited a decreasing thermal conductivity over temperature range of 293 ~ 353 K, and less influenced by pressure. Developing predictive approaches was inevitable as experimental measurements for a wide range of ILs' thermal conductivity were time-consuming and inefficient. Using radial basis function (RBF) network, Mousavi et al.[149] proposed thermal conductivity model based on ILs' thermophysical properties, chemical structures, temperature and pressure from 504 experimental data of 50 ILs. By optimizing the technique with genetic algorithm and gravitational search algorithm, the developed model yields accurate prediction with deviation less than 2%.

3.2. Phase transition of nanoconfined ionic liquids inside capsule shell

With the development of encapsulation technologies, high encapsulation efficiency ($E_{en} = \Delta H_{m,MPCM}/\Delta H_{m,PCM}$, defined as the ratio of melting enthalpy of PCM microcapsule $\Delta H_{m,MPCM}$ and pure PCM $\Delta H_{m,PCM}$) can be reached as high as 90%[150], but most studies exhibit E_{en} limited in the range of 22.5 ~ 69.5 %[14]. Of note, as the most commonly method for IL encapsulation - sol-gel with SiO_2 shell, the E_{en} is even lower with an average value of ~ 51.5%[151-153]. Given the large proportion of capsule shell, it is necessary to evaluate the thermodynamic features of ionic liquids confined inside the shell, as the nanoconfinement effect significantly alter ILs' behavior in the nano-restricted space.

Compared with polymer shells, inorganic shell (i.e. SiO_2, $CaCO_3$, TiO_2) exhibited improved chemical and thermal stability, as well as higher thermal conductivity. SiO_2 is the most commonly utilized shell material in sol-gel encapsulation method. Previous works have shown the mesopores on the surface of SiO_2 shell are detrimental to the leakage proof of liquid PCMs[154, 155]. To eliminate leakage and boost thermal conductivity of the organic shell-composite materials, a usual solution is coating another layer outside SiO_2 shell, but the double layer will undoubtably reduce the enthalpy of encapsulation. Kang et al.[156] double encapsulated paraffin using shells of SiO_2 and graphene sheets/silicone rubber, because the micropores and mesopores on the microcapsule's surface (average pore diameter of 20.35 nm) were a major disadvantage for encapsulation intactness. The pores on the surface of $CaCl_2{\cdot}6H_2O$@SiO_2 also lead to the uniform distribution of $CaCl_2{\cdot}6H_2O$/SiO2 composites[157], and the largest adsorption efficiency could be reached at nano-SiO_2 pore sizes of 15 ± 5 nm. Fig.7a-b showed the SEM images of mesoporous SiO_2 shell and 3D nanoporous TiO_2 layer for PEG encapsulation[158, 159], with average pore diameter of 7.05 nm and 12.12 nm respectively.

A pioneered work of nanoconfined ILs in phase transition was filling [C_4MIM][PF_6]/methanol mixture in multiwalled carbon nanotubes (MWNTs, shown in Fig.7c)[160]. An unexpected high melting temperature was observed, as T_m increases from 6 ℃ for bulk [C_4MIM][PF_6] to 222 ℃ after encapsulation. The good reproducibility of crystallization features of [C_4MIM][PF_6]/methanol@MWNTs encapsulation indicates enhanced thermal stability compared to the bulk system. A series of work have been carried out to understand the confinement effect since then. Ionic liquids trapped in the nanoporous matrices of encapsulation shell belongs to three-dimensional restricted area, which covers the host matrix of metal-organic frameworks [161-163], covalent organic frameworks[164-166], nanoporous silicas (SiO_2)[167, 168] and carbons[169, 170], carbon nanotubes[171-173], zeolites[174-176], etc. Among these porous materials, nanoporous silicas (average pore sizes of 2.0 ~ 34.3 nm) is the most popular one due to their interconnected nanoporous structure, large surface area, high thermal/mechanical stability, nontoxicity and easy synthesis.

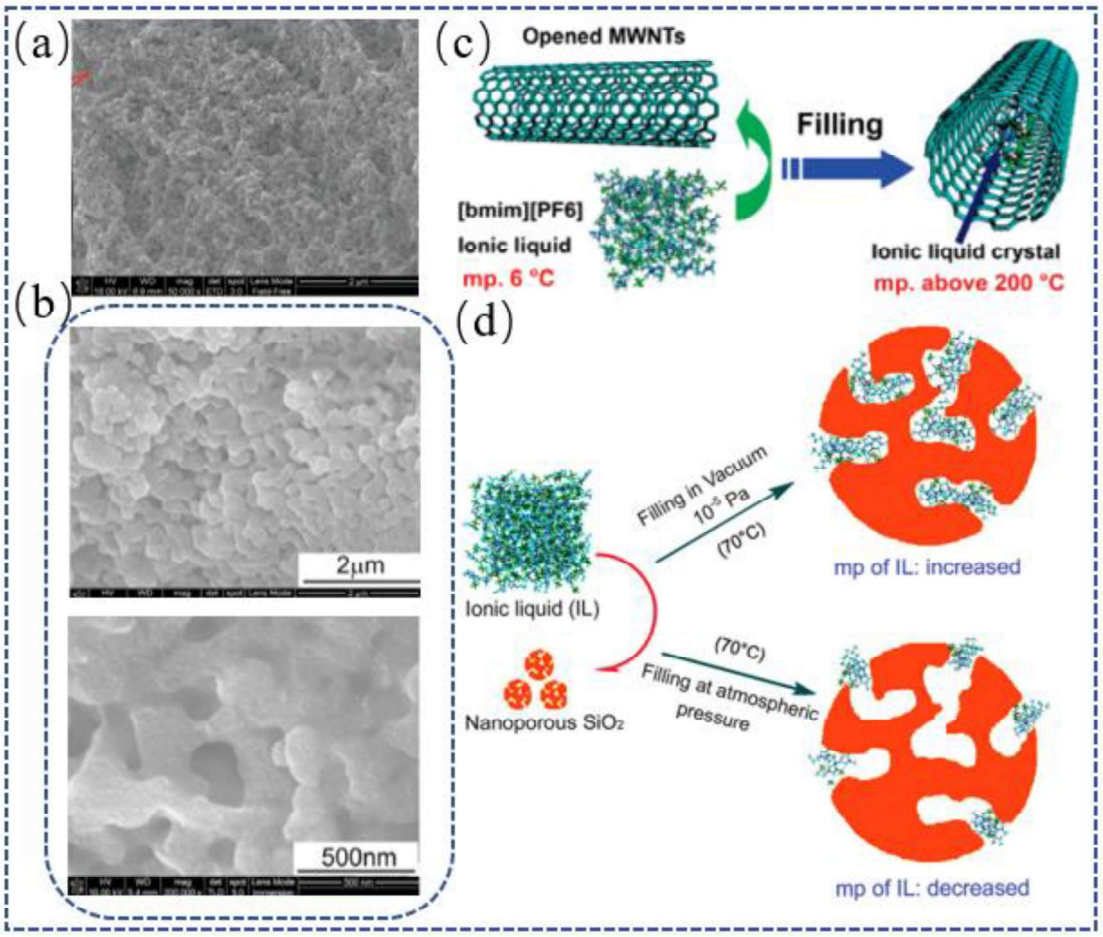

Fig.7. (a) SEM images of mesoporous SiO_2 shell for PEG@SiO_2 encapsulation[159], with the average pore diameter of 7.05 nm; (b) 3D nanoporous TiO_2 layer for PEG@TiO_2 encapsulation[158], the mean pore diameter is 12.12 nm; (c) Schematic of [C_4MIM][PF_6]/methanol encapsulation in open MWNTs[160]; (d) Schematic of change in melting point of ILs entrapped by mesoporous silica under vacuum conditions versus that at atmospheric pressure[177].

The interactions between porous silica and ILs can result in unique properties and behaviour of the confined ILs compared to their bulk counterparts. Near the wall of nanopores, the ILs may be arranged in a 2D ordered pattern with coexistence of liquid-solid phase or in a more disordered liquid-like arrangement[178]. The confinement will therefore lead to a more densified area near the porous surface than the centre domain[179, 180]. This can affect the dynamic properties of ILs (like self-diffusion coefficient, viscosity, thermal conductivity), depending on ILs' molecular structure as well as confining details[181-183]. In terms of imidazolium ILs, the homogeneous electrostatic field caused by cationic part will induce a weak interaction with porous environment, leading to a faster confinement of the cation dynamics than that of

anion[136, 184].

Although plenty of work have shown that nanoconfinement increases ILs' melting point dramatically, the contradictory findings are also frequently reported[70, 185]. The main difference is strictly related to ILs' filling progress[177] as depicted in Fig.7d. Under vacuum conditions, fully loaded nanopores of ILs ensures the confinement effect and strong interaction with silica wall, while complex solid-liquid-gas under atmospheric pressure treatment weaken the nanoconfinement impact and depress the melting point. Previous works have proven the phase transition of confined ILs are sensitive to the cationic/anionic structure, as well as the pore size[186]. As evidenced by an experiment work from Neouze et al.[185], the strong confinement of silica gels depress the melting point of [C_4MI][TFSI] for ~ 10 ℃, or make it disappear under high IL loading ratio, while for [C_2MIM][$OsSO_4$] with large anion demonstrated a greater depression of 52 ℃ than most ILs.

Crystallization kinetics of the bulk and confined IL under isothermal condition can be presented using Avrami method:

$$\log[-\ln(1 - X_t)] = \log K + n \log t \quad (6)$$

where K is the constant of crystallization rate; n is the Avrami exponent relative to the characteristics of nucleation mechanism. Verma and Singh[187] found bulk [C_2MIM][TFSI] shows 3D crystal growth due to multiple Avrami exponent values for varies crystal phases (n = 1.79 ~ 4.1), while the small value of confined ILs (n $\approx$ 1) in silica nanopores indicates one-dimensional crystal growth. Similarly, the isothermal study of pure and silica-confined [C_2MIM][BF_4] showed that confinement feature reduced the speed of ILs' crystallization rate, as K value increases from ~10^{-5} for pure IL to ~ 10^{-4} for nanoconfined IL[188]. Another important parameter is the relative crystallinity (α), referring to the ratio of crystallinity at any time 't' when time approaches infinity[189], and can be expressed as:

$$\alpha = \frac{\Delta H_t}{\Delta H_\infty} = \frac{\int_0^t \frac{dH}{dt} \cdot dt}{\int_0^\infty \frac{dH}{dt} \cdot dt} \quad (7)$$

where dH/dt, ΔH_t and ΔH_∞ is the heating rate, total heat evolution at any time t, and heat

evolved when t approaches infinity (∞), respectively. The crystallization half time, referring to the time consumed to attain 50% crystallization, is sensitive to thermal conductivity of IL and silica matrix. Confined IL takes longer time to crystallize relative to the bulk ILs, attributed to the fact that high thermal conductivity of silica matrix supports faster heat transfer dissipation from IL's crystallization growth[188].

3.3 Nucleation on porous surfaces

Most studies believed that heterogeneous nucleation was always dominant due to the existence of shell and impurities contained in PCMs/ILs. The interface between core and shell provides heterogeneous nucleation sites, resulting in cap-shape solid nucleus rather than sphere shape ones. Considering the fact that the pore size of silicon (5 ~ 12 nm[158, 190], depends on the fabrication progress) is similar to ILs' molecular size (~ 4.2 nm[191]), ILs overcome smaller free energy barrier to nucleate due to the size similarity between substrate surface and nucleation size. As a result, the silicon pores can trap ionic liquid molecules and promote nucleation and crystal growth. Meanwhile, porous surface induces nucleation site for heterogenous nucleation, and promotes nucleation rate compared to that on flat surface. Previous works have shown the nucleation seeds on the porous surface significantly outnumbered that on flat surface, as the fractal structure ensure an adequate molecular concentration for nucleation. Moreover, the chemical attraction between pore surface and ionic molecular can lead to a stronger interaction of IL molecules to the porous surface, which promote a high location concentration and high-density ILs phase. By providing the favorable environment for nucleation, the confinement can ultimately affect crystallization behavior and properties of ILs within the porous materials.

The number of nucleation sites is dramatically influenced by the surface topography of nucleation substrate[192]. To rationalize the texture of porous surface, the fractal dimension is proposed and provide valuable information regarding surface roughness, connectivity of pores and pore size distribution. The nucleation site density, referred as area occupied by all nuclei versus the area occupied by an averaged nucleus[193], can therefore be expressed as:

$$N = \frac{A_R}{\pi \bar{r}_0^2} = \frac{area\ occupied\ by\ all\ nuclei}{area\ occupied\ by\ an\ averaged\ nucleus} \quad (8)$$

where A_R and r0 is the area occupied by all nuclei and average nucleus size, respectively. A simplified form of specific effective nucleation density is proposed depending on the relative size of nuclei and surface element:

$$\log N = m(D-2) + n \tag{9}$$

where $n = -2\log d + \log(4K/\pi)$, d, K, D, m^* is the contact area size, effective ratio ($K \leq 1$), the fractal dimension for materials, surface index, respectively. The fractal dimension is determined by box-counting with side length r, with D = 1 ~ 2 for irregular line or bore surface, or D = 2 ~ 3 for a hexahedron bore surface[192]. As shown in Fig.8, the surface index m can be classified based on the regimes of the contact between the nuclei and substrates:

- m^* = ambient values for D = 2 or d > L_u. L_u and L_i is the up and low bounds of the fractal region, respectively.
- $m^* = \log\left(L_j\big|_{j=u,x}/L_l\right)$ for d < L_l;
- $m^* = \log\left(L_j\big|_{j=u,x}/d\right)$ for L_l < d < L_u. Thus, the nuclei size can be calculated via $d = L_j\big|_{j=u,x}10^{-m}$

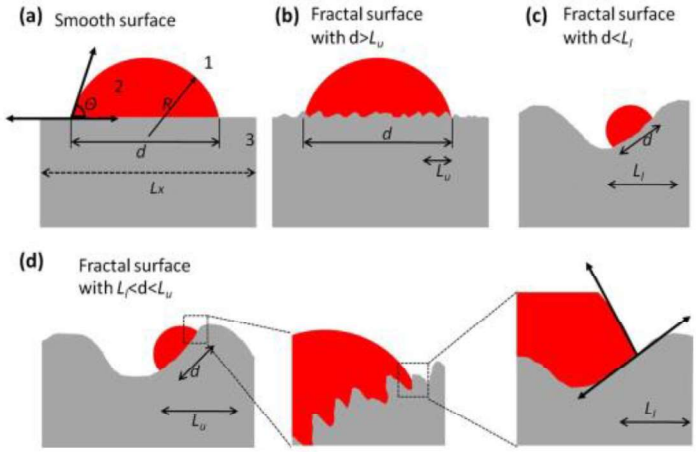

Fig.8. Schematic illustration of heterogeneous nucleation on different surface: (a) nuclei are in contact with smooth surface; (b) d > L_u; (c) d < L_l; (e) L_l < d < L_u; L_u and L_i is the up and low bounds of the fractal region, respectively[193].

Stolyarova et al.[194] studied the enhanced nucleation and crystallization on porous silicon in light of the pore size and shape. They found the nucleation barrier decreases with decreasing

conic angle:

$$\Delta G^*_{pore} = \frac{2}{3}\pi(r^*)^3\gamma_{SL}(1-\cos\alpha/2) = \Delta G^*_{flat}(1-\cos\alpha/2) \quad (10)$$

Where ΔG^*, r^*, γ_{SL} is the potential barrier for nucleation, and radius of the critical nucleus and solid-liquid interface free energy, respectively; α is the conic angle. Regarding encapsulation core, the free energy barrier of heterogenous nucleation can be expressed as:

$$\Delta G^*_{het} = f(m,R^*)\Delta G^*_{homo} = f(m,R^*)\frac{16\pi\gamma^3_{SL}T_m}{3\Delta H(T_m-T)} \quad (11)$$

where ΔG^*_{het} and ΔG^*_{homo} refers to the critical free energy barrier of heterogenous and homogenous nucleation, respectively; $f(m,R^*)$ corresponds to the comprehensive effect induced by the chemical parameters and surfaces topography on reducing the free energy barrier; m is relative to the contact angle of liquid and solid nucleis; $\gamma_{SL}$and ΔH is the interface energy between liquid and solid, and volumetric enthalpy of PCM fusion, respectively. The facto R* ($R^* = R/r_c$, ratio of surface radius and critical size of nucleis) and the geometry factor f for the convex nanoroughness can be given as:

$$f(m,R^*) = \frac{1}{2}+\frac{1}{2}\left(1-\frac{mR^*}{\omega}\right)^3+\frac{1}{2}R^{*3}\left[2-\frac{3(R^*-m)}{\omega}+\left(\frac{(R^*-m)}{\omega}\right)^3\right]+\frac{3}{2}mR^{*3}\left[\frac{(R^*-m)}{\omega}-1\right] \quad (12)$$

where $w = \left(1+R^{*2}-2mR^*\right)^{1/2}$. Similarly, for concave nanoroughness the geometry factor can be given as:

$$f(m,R^*) = \frac{1}{2}-\frac{1}{2}\left(1+\frac{mR^*}{\omega}\right)^3-\frac{1}{2}R^{*3}\left[2-\frac{3(R^*+m)}{\omega}+\left(\frac{(R^*+m)}{\omega}\right)^3\right] + \frac{3}{2}mR^{*3}\left[\frac{(R^*+m)}{\omega}-1\right] \quad (13)$$

where $= \left(1+R^{*2}-2mR^*\right)^{1/2}$. Then the heterogeneous nucleation rate can be given as follows:

$$J_{het} = A_{het}exp\left[-\frac{f(m,R^*)\Delta G^*_{homo}}{k_BT}\right] \quad (14)$$

ere A_{het} is the nucleation pre-factor. Futhermore, the heterogeneous nucleation rate can also be

determined by counting counting the number of nucleation events occurring at a supercooled temperature[195]:

$$J_{het}(T_i) = \frac{Rn_i}{S_m \Delta T_i \left(n_i/2 + \sum_{j>i} n_j\right)} \quad (15)$$

where R is the cooling rate (K/s), S is the specific surface area of the sample ($m^2\ g^{-1}$), m is the mass of the sample (g), ΔT_i is the width of the ith temperature bin centered at T_i, and n_i is the number of freezing events occurring in the temperature range ΔT_i.

Conclusively, although crystallization behavior of nanoconfined IL filled in silica matrix has been widely studied, its effect on IL@silica encapsulation is still lack of study – Does ILs still leak via porous shell given their high viscosity? How does the nanoconfined ILs in porous shell affect encapsulation's overall phase transition features? Whether there is a critical shell proportion that the nanoconfined effect can be ignored in terms of encapsulation's overall performance? Moreover, the crystallization and nucleation mechanism of ILs on porous surface still lack of systematically studied. Therefore, more efforts should be devoted to these inevitable and crucial problems so that encapsulation's geometry features and energy storage capability can be optimized.

4. Application prospect of ionic liquids-based phase change materials

***Infrared stealthy*:** In the field of military technology, reducing the surface temperature is one of the effective methods to reduce the infrared thermal radiation and avoid detection, which could be achieved by applying thermal insulation material on the surface. Sun et al.[196] fabricated mid-infrared films to control the integrated emissivity by doped IL of [C_6MIM][NTf_2] with MWCNT thin film (shown in Fig.9a). The functional films exhibited thermal emissivity of 0.15 ~ 0.7 by IL gating and excellent stability, reaching 3500 cycles with 95% modulation retention. The IL's anionic intercalation and ionic adsorption on MWCNTs contributed to the enhanced electrical conductivity, leading to decreased emissivity of the films within the intermediate infrared spectral range. With intercalation/deintercalation of [DEME][TFSI], Zhao et al.[197] modulate the surface infrared emissivity (0.41~ 0.57) based on the intercalation principle. By embedding graphene in [C_4MIM][BF_6], Ergoktas et al.[198] prepared a new class

of infrared textile devices for future application of complex infrared stealth fabric. Chen et al. [199] embedded long-chain alkyl imidazole ionic liquids to thermoplastic polyurethane prepare infrared camouflage device that can adjust temperature and emissivity. As shown in Fig.9b, the composites exhibited good thermal stability without any enthalpy changes after hundreds of thermal cycles, which provide effective guidance for thermal camouflage in new military equipment. There are, however, still technical deficiencies like permeation of overdose ILs, prolongation of response time after IL degradation, mechanical strength and aging resistance to be optimized for better performance[200].

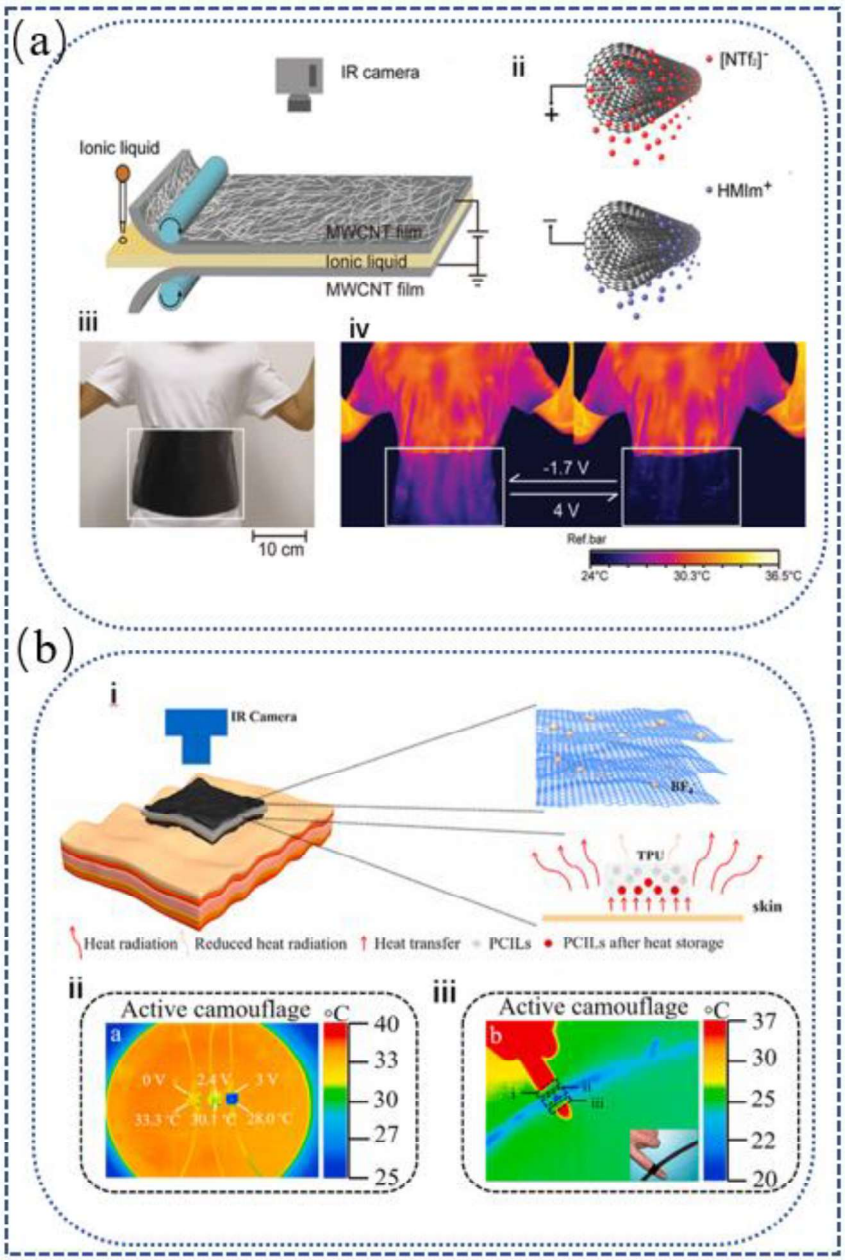

Fig.9. (a) Fabrication and thermal camouflage of the MWCNT-based mid-infrared modulator[196]: (i) and (ii) Schematic of the roll-to-roll process to fabricate a sandwich-structured MWCNT/IL-Celgard/MWCNT film; (iii) Optical image of a flexible large-area functional film adhered to hum waist; (iv) Thermal images of the as-fabricated film with negative (~ 1.7 V) and positive voltages (4V), respectively. (b) Fabrication process of the flexible phase-change stealthy material: (i) main steps of preparing MLG/PCILs; (ii) Thermal images of MLG/PCIL at 0V, 2.4V and 3V, respectively; (iii) Thermal infrared camouflage application on finger.

***Solar thermal utilization*:** Although traditional PCMs have been utilized in energy system to overcome the disadvantages of seasonal and nonuniform regional distribution of solar energy, their overall heat and release efficiency were only 40.4% and 4.2% respectively. As demonstrated in Table 1, the sensible energy storage density and thermal conductivity of imidazolium ILs are higher than that of commercial media, thus they can replace traditional PCMs and utilized in parabolic solar collators. Das et al.[57] found the energy storage density of imidazolium ILs can satisfy the minimum required value of solar energy system (>1.9 MJ/($m^3 \cdot K^{-1}$)). Tang et al.[201] used a novel pseudo ionic liquid PCMs in solar water heating system, which exhibited excellent thermal stability with latent enthalpy of 174.9 kJ/kg upon melting at 86.9 ℃. The photothermal properties of ILs can be further improved by adding slight amount of optical sensitive materials. As shown in Fig. 10a, Liu et al.[202] utilized a graphene/[HMIM]BF4 ionic liquid nanofluid as an absorber in high-temperature direct solar collectors, and proposed a model formula for IL-based volumetric solar receiver (-80 ~ 340 ℃). To further elevate ILs' performance, Chereches et al.[203] discussed the application possibility of hybrid ILs for solar thermal utilization. They found the energy storage density of two hybrid materials was improved up to 284% respectively relative to Thermonal VP-1. Moreover, with the aid of computer-aided ionic liquid design (CAILD) model, Mehrkesh and Karunanithi[204] utilized optimal ILs consisting of a hydroxyl-functionlized imidazolium cation and tetrafluoroborate anion as thermal storage medium, as given in Fig.10b. The designed IL has a higher thermal storage capacity than commercial oil and molten salt, and the corresponding required volume is lowest to store a given amount of thermal energy.

***Thermal management in extreme environment*:** Functional ILs with elevated heat enthalpy and decomposition temperature are preferred for heat management systems in extreme space

environments. The main challenges of outer space are solar radiation and extreme cold/heat thermal control requirement for manned spacecraft. To tackle these challenges, functional ILs based composition were promoted, which exhibit a high heat of fusion (> 200 kJ/kg) upon transition temperature range of 8 to 12 ℃. The absence of corrosiveness or phase degradation during solid-liquid transition is another advantage of these ILs[205]. Their enhanced properties such as higher thermal conductivity, heat fusion, or thermal diffusivity allow for more efficient heat transfer within the thermal system, resulting in reduction in size and weight of corresponding heat exchangers[56], as given in Fig.10c. Therefore, functional ILs is a promising choice for thermal control in manned spacecraft or other applications requiring efficient heat management.

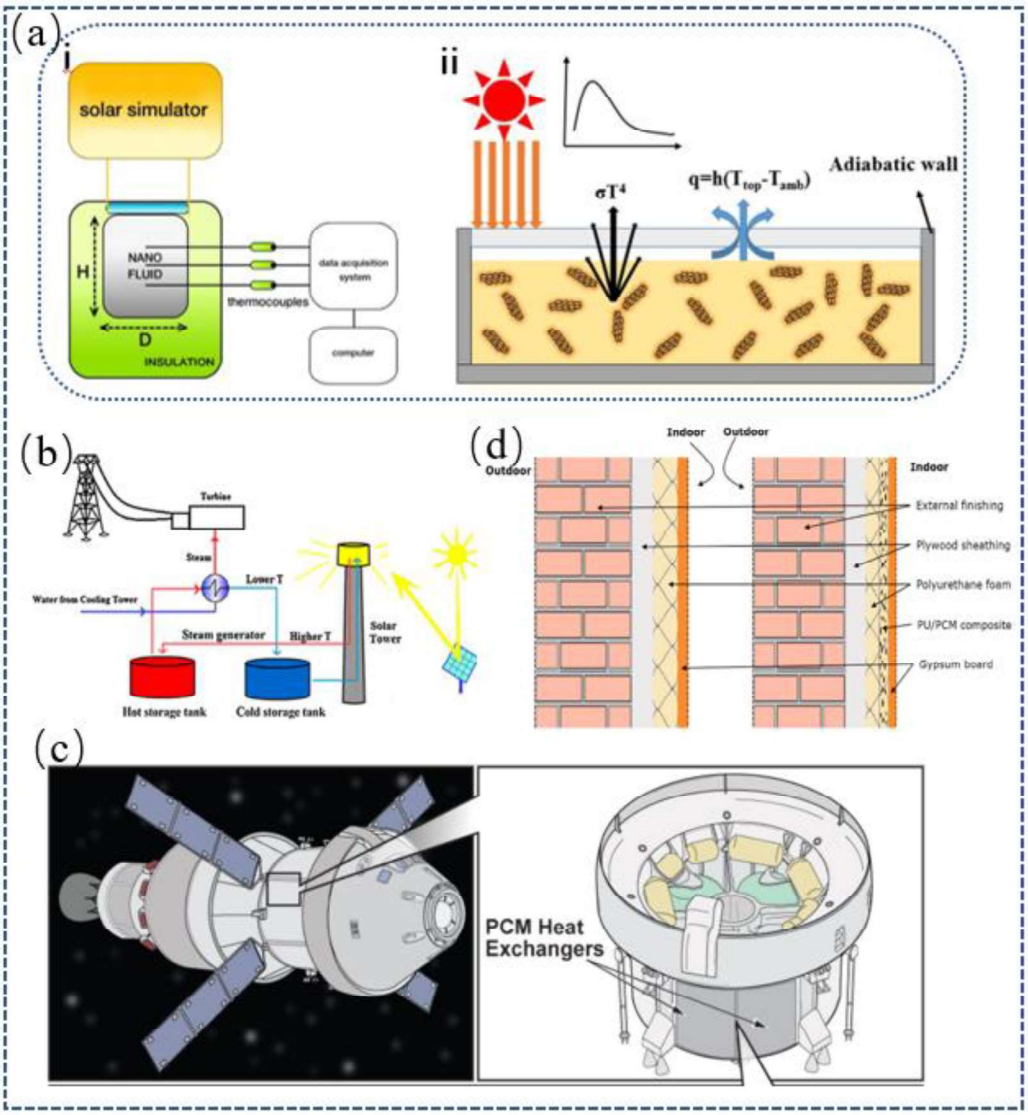

Fig.10. (a) Schematic of direct solar collector and model formulation of a graphene/[HMIM]BF_4 based volumetric solar receiver[202]. (b) Schematic of a solar energy storage system using imidazolium ionic liquid as thermal storage medium[204]; (c) Low Temperature IonoTherm Phase Change Material Heat Exchanger[56]; (d) Comparison of building assembly conventional wall and wall with an additional PCM composite layer[206].

***Green energy-saving building*:** PCM-based energy storage technology has been proved to be environment-friendly in buildings with less electrical demanding, because conventionally electricity should be consumed to heat up building interior with radiators or cool down with air-conditioning. As shown in Fig.10d, PCMs upon melting at 18 ~ 30 ℃ were utilized in buildings to investigate their impact of surrounding temperature, types/locations on energy saving efficiency of buildings[206]. Many imidazolium ILs are reported as nontoxicity and can be used in building applications[207]. The IL-water hybrid performs better than tradition H_2O/LiBr solution - H_2O/[C_{10}MIM][DMP] has the highest coefficient of performance (COP) above generation temperature of 86 ℃[208], while H_2O/[C_2MIM][$EtSO_4$] yields the highest COP below temperature of 75 ℃. However, high viscosities still hindered the application of ILs and future efforts should be devoted to reduce system pressure drop by heat/mass transfer enhancement or system optimization.

7. Conclusion and prospects

Due to their rich crystallization behavior and wide thermal 'tailor-made' properties, ionic liquids can be treated as the missing link between conventional PCMs and high-temperature molten salts for renewable thermal energy storage. Among the various IL families, imidazolium-based ILs have been frequently reported due to low vapor pressure, high conductivity in spite of high viscosity. Indeed, plenty of data have been reported on ILs' properties like viscosity/density, and while relationship regarding structure-property is included, data on the phase transition behavior is scarcely reported, and drawbacks of supercooling and low enthalpy still hinder ILs' widespread application. In this regard, present work summarized the methods of supercooling regulation and enthalpy elevation of imidazolium ILs firstly, and proposed method of IL encapsulation with crystallization-promoting porous shell to reduce the effectively viscosity, avoid solid-liquid transition leakage, decreasing phase separation and

supercooling. Then the phase transition behavior of ILs within capsule core and nanoconfined ILs inside the capsule shell, as well as the nucleation features on porous shell surface were given. Furthermore, the practical applications of imidazolium ILs and microencapsulation were reported.

Conclusion drawn by the review. (1) Main defects of imidazolium ILs as PCMs are low enthalpy and supercooling. Due to the cage-like structure, ILs immiscible with both non-polar aromatic materials and the polar aromatics. Therefore, semi-crystalline polymer PEG with high enthalpy can be used to form "hybrid green" composition to elevate efficient heat enthalpy. In terms of supercooling, the metastable state can be suppressed or eliminated by enhancing heterogeneous nucleation inside encapsulation. Porous shell not only significantly alter dynamic properties of ILs (lifting T_m from 6 to 222 ℃) inside confined nanoporous, but also induces more seeding sites for heterogeneous nucleation. The silicon pore size is similar to the molecular size of ILs, and the pores may trap ILs' molecular and promote nucleation rate on the surface of porous shell. However, precious control of shell's nano-structure during ILs' encapsulation fabrication is scarily reported, and mechanism of crystallization-promoting pathway on porous surface should be further explored.

(2) Imidazolium ILs have a wide range of melting temperature of - 87 ~ 208 ℃ with heat enthalpy of 59.00 ~ 152.56 kJ/kg, as well as several advantages such as antiseptic, anticorrosion, dampness and gas composition adjustment. These properties make them idea energy materials for cold chain logistics. However, their phase transition mechanisms are rather complex, not only heated/cooled rate but also the initial state of the studied IL influence rather significantly. Under high cooling rates, the alkyl chain rotational motions become randomly frozen, leading to a nonequilibrium condition that hinder IL nucleation. Under low cooling rates, the collective motions of cationic alkyl are stimulated, but the thermal excited rational pattern are restrained. This results in the formation of randomly distributed nanocrystal within the ILs. Furthermore, the length of alkyl chain and ILs' substituents strongly influence their internal forces, including hydrogen bond, coulomb force, van der Waals force, functional group, electrostatic force, symmetry, and other factors among ions. These factors can cause variations in melting and decomposition temperature of imidazolium ILs.

Future perspectives. (1) The thermal repeatability of imidazolium ILs should be presented as materials only subjected to several heating/cooling cycles in previous work, while commercial PCMs usually require stability upon thousands of repeated charging and discharging processes. This is especially important for the composited ILs (binary ILs or with PEG), where phase separation or supercooling might get worse. In repeatability tests, annealing condition (temperature and lasting time) should be carefully treated as it shows a significant thermal effect on crystallization condition. In terms of thermal stability, decomposition temperature derived from TGA measurement is not reliable due to interference factors like sample pan materials, atmosphere type and flow rate, which makes comparisons to literature values difficult. Accurate measurement from UV-Vis or fluorescence spectroscopy can be obtained as they capture chemical changes of ILs' decomposition, yielding values 140 ℃ lower than that of TGA.

(2) Although supercooling is usually treated as disadvantage for PCMs, it however may be beneficial to the seasonal heat storage. In a pioneer work, Schultz et al.[209] proposed large supercooling allows storage part to cool to the ambient temperature without undergoing solidification. This means the part of storage will not experience heat loss but still retains latent heat. Inspired by that, Bai et al.[210] proposed [C_{16}MIM]Br as proper energy materials due to excellent heat of fusion (152.56 kJ/kg) and stable supercooling (20 ℃) with addictive of graphite powder or copper powder. Following work was lagged by the high price and single supercooling regulation method. With the mature of IL synthesize progress, their price has largely reduced and precious control of supercooling can be realized. Therefore, actively utilization of ILs' supercooling for seasonal energy storage is very promising in the future.

(3) The application of ILs as PCMs is still largely in the laboratory stage, while less effort was devoted on their practical applications. One of the main challenges is that the current industry equipment is accustomed to using conventional thermal fluids, and transitioning to ILs would require a significant initial investment. Further research and development efforts are needed to explore alternative IL compositions beyond the commonly studied imidazolium, pyridine, quaternary ammonium, pyrrolidine cationic salts with halogen, and anionic liquids ($[BF_4]^-$, $[PF_6]^-$ and $[Tf_2N]^-$). To make ILs more viable for practical application, it is important to focus on developing functional ILs that are cost-effective and exhibit thermal performance. By

addressing these challenges and further advancing the understanding of ILs, it may be possible to overcome the hurdles of practical implementation and pave the way for broader use of ILs as PCMs in various industries.

Acknowledgements

The authors acknowledge the funding supports from National key research and development program of China (2023YFB2406500), Beijing Natural Science Foundation (3222026), high-end talents development program (049000514123546) of Beijing University of Technology.

CRediT authorship contribution statement

All authors have participated in (a) conception and design, or analysis and interpretation of the data; (b) drafting the article or revising it critically for important intellectual content; and (c) approval of the final version.

Declaration of competing interest

This manuscript has not been submitted to, nor is under review at, another journal or other publishing venue. The authors have no affiliation with any organization or indirect financial interest in the subject matter discussed in the manuscript.

Data availability

No data was used for the research described in the article.

References

[1] Gil, A, M Medrano, I Martorell, A Lázaro, P Dolado, B Zalba, L F Cabeza, State of the art on high temperature thermal energy storage for power generation. Part 1—Concepts, materials and modellization. *Renewable and Sustainable Energy Reviews*, **2010**. 14(1): 31-55.

[2] Medrano, M, A Gil, I Martorell, X Potau, L F Cabeza, State of the art on high-temperature thermal energy storage for power generation. Part 2—Case studies. *Renewable and Sustainable Energy Reviews*,

2010. 14(1): 56-72.
[3] International Vaccine Access Center (IVAC), Johns Hopkins Bloomberg School of Public Health. VIEW-hub. https://view-hub.org/covid-19/characteristics, **2023**: [Accessed: 2023/11/16].
[4] Yin, Z, J Zheng, H Kim, Y Seo, P Linga, Hydrates for cold energy storage and transport: A review. *Advances in Applied Energy*, **2021**. 2: 100022.
[5] Xie, P, L Jin, G Qiao, C Lin, C Barreneche, Y Ding, Thermal energy storage for electric vehicles at low temperatures: Concepts, systems, devices and materials. *Renewable and Sustainable Energy Reviews*, **2022**. 160: 112263.
[6] Jankowski, N R, F P McCluskey, A review of phase change materials for vehicle component thermal buffering. *Applied Energy*, **2014**. 113: 1525-1561.
[7] Hua, W, L Zhang, X Zhang, Research on passive cooling of electronic chips based on PCM: A review. *Journal of Molecular Liquids*, **2021**. 340: 117183.
[8] Singh, S, K K Gaikwad, Y S Lee, Phase change materials for advanced cooling packaging. *Environmental Chemistry Letters*, **2018**. 16(3): 845-859.
[9] B, K, A K Pandey, S Shahabuddin, M Samykano, T M, R Saidur, Phase change materials integrated solar thermal energy systems: Global trends and current practices in experimental approaches. *Journal of Energy Storage*, **2020**. 27: 101118.
[10] Liu, Y, R Zheng, J Li, High latent heat phase change materials (PCMs) with low melting temperature for thermal management and storage of electronic devices and power batteries: Critical review. *Renewable and Sustainable Energy Reviews*, **2022**. 168: 112783.
[11] Pereira da Cunha, J, P Eames, Thermal energy storage for low and medium temperature applications using phase change materials – A review. *Applied Energy*, **2016**. 177: 227-238.
[12] Hameed, G, M A Ghafoor, M Yousaf, M Imran, M Zaman, A Elkamel, A Haq, M Rizwan, T Wilberforce, M A Abdelkareem, A G Olabi, Low temperature phase change materials for thermal energy storage: Current status and computational perspectives. *Sustainable Energy Technologies and Assessments*, **2022**. 50: 101808.
[13] Eanest Jebasingh, B, A Valan Arasu, A detailed review on heat transfer rate, supercooling, thermal stability and reliability of nanoparticle dispersed organic phase change material for low-temperature applications. *Materials Today Energy*, **2020**. 16: 100408.
[14] Peng, H, D Zhang, X Ling, Y Li, Y Wang, Q Yu, X She, Y Li, Y Ding, n-Alkanes Phase Change Materials and Their Microencapsulation for Thermal Energy Storage: A Critical Review. *Energy & Fuels*, **2018**. 32(7): 7262-7293.
[15] Venkatraman, V, S Evjen, H K Knuutila, A Fiksdahl, B K Alsberg, Predicting ionic liquid melting points using machine learning. *Journal of Molecular Liquids*, **2018**. 264: 318-326.
[16] Earle, M J, K R Seddon, Ionic liquids. Green solvents for the future. *Pure and Applied Chemistry*, **2000**. 72(7): 1391-1398.
[17] Zhou, T, C Gui, L Sun, Y Hu, H Lyu, Z Wang, Z Song, G Yu, Energy Applications of Ionic Liquids: Recent Developments and Future Prospects. *Chemical Reviews*, **2023**. 123(21): 12170-12253.
[18] Mezger, M, H Schröder, H Reichert, S Schramm, J S Okasinski, S Schöder, V Honkimäki, M Deutsch, B M Ocko, J Ralston, M Rohwerder, M Stratmann, H Dosch, Molecular layering of fluorinated ionic liquids at a charged sapphire (0001) surface. *Science*, **2008**. 322(5900): 424-8.
[19] Welton, T, Room-Temperature Ionic Liquids. Solvents for Synthesis and Catalysis. *Chemical Reviews*, **1999**. 99(8): 2071-2084.
[20] Piper, S L, M Kar, D R MacFarlane, K Matuszek, J M Pringle, Ionic liquids for renewable thermal

energy storage – a perspective. *Green Chemistry*, **2022**. 24(1): 102-117.
[21] Valkenburg, M E V, R L Vaughn, M Williams, J S Wilkes, Thermochemistry of ionic liquid heat-transfer fluids. *Thermochimica Acta*, **2005**. 425(1): 181-188.
[22] Baetens, R, B P Jelle, A Gustavsen, Phase change materials for building applications: A state-of-the-art review. *Energy and Buildings*, **2010**. 42(9): 1361-1368.
[23] Zhu, J, L Bai, B Chen, W Fei, Thermodynamical properties of phase change materials based on ionic liquids. *Chemical Engineering Journal*, **2009**. 147(1): 58-62.
[24] Mora, S, G Neculqueo, R A Tapia, J I Urzúa, Thermal storage density of ionic liquid mixtures: A preliminary study as thermal fluid. *Journal of Molecular Liquids*, **2019**. 282: 221-225.
[25] Touazi, A A, S Didaoui, K Khimeche, M Rial, S A Moulaï, M Benziane, Experimental and theoretical studies of volumetric and viscous properties of n-tetradecane with isomeric pentanols. *Journal of Molecular Liquids*, **2021**. 327: 114860.
[26] Zheng, X, Y Bao, D Qu, J Wu, G Qin, Y Liu, Thermal conductivity measurements for long-chain n-alkanes at evaluated temperature and pressure: n-dodecane and n-tetradecane. *The Journal of Chemical Thermodynamics*, **2021**. 162: 106566.
[27] Beil, S, M Markiewicz, C S Pereira, P Stepnowski, J Thöming, S Stolte, Toward the Proactive Design of Sustainable Chemicals: Ionic Liquids as a Prime Example. *Chemical Reviews*, **2021**. 121(21): 13132-13173.
[28] Ge, R, C Hardacre, P Nancarrow, D W Rooney, Thermal Conductivities of Ionic Liquids over the Temperature Range from 293 K to 353 K. *Journal of Chemical & Engineering Data*, **2007**. 52(5): 1819-1823.
[29] Rooney, D, J Jacquemin, R Gardas, *Thermophysical Properties of Ionic Liquids*, in *Ionic Liquids*, B Kirchner, Editor. 2010, Springer Berlin Heidelberg: Berlin, Heidelberg. p. 185-212.
[30] Maton, C, N De Vos, C V Stevens, Ionic liquid thermal stabilities: decomposition mechanisms and analysis tools. *Chemical Society Reviews*, **2013**. 42(13): 5963-5977.
[31] Zhang, H, W Xu, J Liu, M Li, B Yang, Thermophysical properties of dicationic imidazolium-based ionic compounds for thermal storage. *Journal of Molecular Liquids*, **2019**. 282: 474-483.
[32] Zhang, H, M Li, B Yang, Design, Synthesis, and Analysis of Thermophysical Properties for Imidazolium-Based Geminal Dicationic Ionic Liquids. *The Journal of Physical Chemistry C*, **2018**. 122(5): 2467-2474.
[33] Liu, J, W Yang, Z Li, F Ren, H Hao, Experimental investigation of thermo-physical properties of geminal dicationic ionic compounds for latent thermal energy storage. *Journal of Molecular Liquids*, **2020**. 307: 112994.
[34] Zhang, Z, A A M Salih, M Li, B Yang, Synthesis and Characterization of Functionalized Ionic Liquids for Thermal Storage. *Energy & Fuels*, **2014**. 28(4): 2802-2810.
[35] Fabre, E, S M S Murshed, A review of the thermophysical properties and potential of ionic liquids for thermal applications. *Journal of Materials Chemistry A*, **2021**. 9(29): 15861-15879.
[36] Rodil, E, A Arce, A Arce, A Soto, Measurements of the density, refractive index, electrical conductivity, thermal conductivity and dynamic viscosity for tributylmethylphosphonium and methylsulfate based ionic liquids. *Thermochimica Acta*, **2018**. 664: 81-90.
[37] Shevelyova, M P, Y U Paulechka, G J Kabo, A V Blokhin, A G Kabo, T M Gubarevich, Physicochemical Properties of Imidazolium-Based Ionic Nanofluids: Density, Heat Capacity, and Enthalpy of Formation. *The Journal of Physical Chemistry C*, **2013**. 117(9): 4782-4790.
[38] Yusoff, R, A Shamiri, M K Aroua, A Ahmady, M S Shafeeyan, W S Lee, S L Lim, S N M

Burhanuddin, Physical properties of aqueous mixtures of N-methyldiethanolamine (MDEA) and ionic liquids. *Journal of Industrial and Engineering Chemistry*, **2014**. 20(5): 3349-3355.
[39] Nieto de Castro, C A, M J V Lourenço, A P C Ribeiro, E Langa, S I C Vieira, P Goodrich, C Hardacre, Thermal Properties of Ionic Liquids and IoNanofluids of Imidazolium and Pyrrolidinium Liquids. *Journal of Chemical & Engineering Data*, **2010**. 55(2): 653-661.
[40] Yebra, F, J Troncoso, L Romaní, Thermal conductivity of ionic liquids under pressure. *Fluid Phase Equilibria*, **2020**. 515: 112573.
[41] Wang, B, X Wang, W Lou, J Hao, Ionic liquid-based stable nanofluids containing gold nanoparticles. *Journal of Colloid and Interface Science*, **2011**. 362(1): 5-14.
[42] Domańska, U, Thermophysical properties and thermodynamic phase behavior of ionic liquids. *Thermochimica Acta*, **2006**. 448(1): 19-30.
[43] Efimova, A, G Hubrig, P Schmidt, Thermal stability and crystallization behavior of imidazolium halide ionic liquids. *Thermochimica Acta*, **2013**. 573: 162-169.
[44] Shi, H, X Zhang, K Sundmacher, T Zhou, Model-based optimal design of phase change ionic liquids for efficient thermal energy storage. *Green Energy & Environment*, **2021**. 6(3): 392-404.
[45] Zhang, H, J Liu, M Li, B Yang, Functional groups in geminal imidazolium ionic compounds and their influence on thermo-physical properties. *Journal of Molecular Liquids*, **2018**. 269: 738-745.
[46] Liu, J, F Wang, L Zhang, X Fang, Z Zhang, Thermodynamic properties and thermal stability of ionic liquid-based nanofluids containing graphene as advanced heat transfer fluids for medium-to-high-temperature applications. *Renewable Energy*, **2014**. 63: 519-523.
[47] He, G, X Fang, T Xu, Z Zhang, X Gao, Forced convective heat transfer and flow characteristics of ionic liquid as a new heat transfer fluid inside smooth and microfin tubes. *International Journal of Heat and Mass Transfer*, **2015**. 91: 170-177.
[48] Chen, W, C Zou, X Li, An investigation into the thermophysical and optical properties of SiC/ionic liquid nanofluid for direct absorption solar collector. *Solar Energy Materials and Solar Cells*, **2017**. 163: 157-163.
[49] Valderrama, J O, L F Cardona, Predicting the melting temperature and the heat of melting of ionic liquids. *Journal of Ionic Liquids*, **2021**. 1(1): 100002.
[50] Čanji, M, M Bendová, M G Bogdanov, Z Wagner, N Zdolšek, F Quirion, V Jandová, P Vrbka, Phase transitions in higher-melting imidazolium-based ionic liquids: Experiments and advanced data analysis. *Journal of Molecular Liquids*, **2019**. 292: 111222.
[51] Liu, Y, Z Dai, Z Zhang, S Zeng, F Li, X Zhang, Y Nie, L Zhang, S Zhang, X Ji, Ionic liquids/deep eutectic solvents for CO2 capture: Reviewing and evaluating. *Green Energy & Environment*, **2021**. 6(3): 314-328.
[52] Cao, Y, Y Chen, X Sun, Z Zhang, T Mu, Water sorption in ionic liquids: kinetics, mechanisms and hydrophilicity. *Physical Chemistry Chemical Physics*, **2012**. 14(35): 12252-12262.
[53] Siddiquee, M A, R Patel, J Saraswat, B S Khatoon, M ud din Parray, F A Wani, M R Khan, R Busquets, Interfacial and antibacterial properties of imidazolium based ionic liquids having different counterions with ciprofloxacin. *Colloids and Surfaces A: Physicochemical and Engineering Aspects*, **2021**. 629: 127474.
[54] Jagadeeswara Rao, C, K A Venkatesan, B V R Tata, K Nagarajan, T G Srinivasan, P R Vasudeva Rao, Radiation stability of some room temperature ionic liquids. *Radiation Physics and Chemistry*, **2011**. 80(5): 643-649.
[55] Qi, W, M Li, L Zhao, Effect of radiation on interfacial properties and phase behavior of ionic liquid-

based microemulsions. *Radiation Physics and Chemistry*, **2020**. 168: 108596.
[56] Asha, S, D Thomas, K P Vijayalakshmi, B K George, Thermal decomposition of N-butyl-N-methyl pyrrolidinium tetrafluoroborate and N-butyl-N-methyl pyrrolidinium hexafluorophosphate: Py-GC–MS and DFT study. *Journal of Molecular Liquids*, **2021**. 333: 115978.
[57] Das, L, F Rubbi, K Habib, N Aslfattahi, R Saidur, B Baran Saha, S Algarni, K Irshad, T Alqahtani, State-of-the-art ionic liquid & ionanofluids incorporated with advanced nanomaterials for solar energy applications. *Journal of Molecular Liquids*, **2021**. 336: 116563.
[58] Bakthavatchalam, B, K Habib, R Saidur, B B Saha, K Irshad, Comprehensive study on nanofluid and ionanofluid for heat transfer enhancement: A review on current and future perspective. *Journal of Molecular Liquids*, **2020**. 305: 112787.
[59] Bo, L, X Zhang, Z Luo, T Saboori, M Dehghan, M Ghasemizadeh, H Karimi-Maleh, A Alagumalai, O Mahian, An overview of the applications of ionic fluids and deep eutectic solvents enhanced by nanoparticles. *Journal of Thermal Analysis and Calorimetry*, **2022**. 147(14): 7589-7601.
[60] Matuszek, K, C Hatton, M Kar, J M Pringle, D R MacFarlane, Molecular patterns in the thermophysical properties of pyridinium ionic liquids as phase change materials for energy storage in the intermediate temperature range. *Journal of Non-Crystalline Solids: X*, **2022**. 15: 100108.
[61] Matuszek, K, M Kar, J M Pringle, D R MacFarlane, Phase Change Materials for Renewable Energy Storage at Intermediate Temperatures. *Chemical Reviews*, **2023**. 123(1): 491-514.
[62] Urzúa, J I, M L Valenzuela, J Cavieres, M J Inestrosa-Izurieta, Ionic liquid mixtures as energy storage materials: a preliminary and comparative study based on thermal storage density. *RSC Advances*, **2023**. 13(28): 19412-19419.
[63] Nasirpour, N, M Mohammadpourfard, S Zeinali Heris, Ionic liquids: Promising compounds for sustainable chemical processes and applications. *Chemical Engineering Research and Design*, **2020**. 160: 264-300.
[64] Triolo, A, A Mandanici, O Russina, V Rodriguez-Mora, M Cutroni, C Hardacre, M Nieuwenhuyzen, H-J Bleif, L Keller, M A Ramos, Thermodynamics, Structure, and Dynamics in Room Temperature Ionic Liquids: The Case of 1-Butyl-3-methyl Imidazolium Hexafluorophosphate ([bmim][PF6]). *The Journal of Physical Chemistry B*, **2006**. 110(42): 21357-21364.
[65] Cui, W, X Li, X Li, L Lu, T Ma, Q Wang, Combined effects of nanoparticles and ultrasonic field on thermal energy storage performance of phase change materials with metal foam. *Applied Energy*, **2022**. 309: 118465.
[66] Zhang, H, C Xu, G Fang, Encapsulation of inorganic phase change thermal storage materials and its effect on thermophysical properties: A review. *Solar Energy Materials and Solar Cells*, **2022**. 241: 111747.
[67] Zhao, Y, X Zhang, X Xu, S Zhang, Research progress in nucleation and supercooling induced by phase change materials. *Journal of Energy Storage*, **2020**. 27: 101156.
[68] Matsumoto, K, J Ueda, K Ehara, J Sakamoto, Y Furudate, Active control of supercooling degree using two surfactants of different molecular sizes. *International Journal of Refrigeration*, **2018**. 85: 462-471.
[69] Xu, T, A Zhang, Y Zhao, Z Han, L Xue, Crystallization kinetics and morphology of biodegradable poly(lactic acid) with a hydrazide nucleating agent. *Polymer Testing*, **2015**. 45: 101-106.
[70] Singh, V, K D Amirchand, R L Gardas, Ionic liquid-nanoparticle based hybrid systems for energy conversion and energy storage applications. *Journal of the Taiwan Institute of Chemical Engineers*, **2022**. 133: 104237.

[71] Iwase, K, Y Hikita, I Yoshikawa, H Houjou, K Ishino, Molecular Structural Insight into the Cold Crystallization Process of Ionic Liquid Crystals. *The Journal of Physical Chemistry C*, **2022**. 126(26): 10668-10676.
[72] Fu, D, Y Liu, Y Su, G Liu, D Wang, Crystallization Behavior of Binary Even−Even n-Alkane Mixtures in Microcapsules: Effect of Composition and Confined Geometry on Solid−Solid phase Separation. *The Journal of Physical Chemistry B*, **2011**. 115(16): 4632-4638.
[73] Tanaka, D, R Hijiya, T Wakamatsu, The effects of applying an alternating electric field to lysozyme solutions during the initial crystallization stage. *Journal of Crystal Growth*, **2021**. 573: 126288.
[74] Kang, T, Y You, R Hoptowit, M M Wall, S Jun, Effect of an oscillating magnetic field on the inhibition of ice nucleation and its application for supercooling preservation of fresh-cut mango slices. *Journal of Food Engineering*, **2021**. 300: 110541.
[75] Yuan, Y, X Jiang, S Poddar, X Xu, Electric-field assisted nucleation processes of croconic acid films. *CrystEngComm*, **2019**. 21(48): 7460-7467.
[76] Arshad, A, M Jabbal, H Faraji, P Talebizadehsardari, M A Bashir, Y Yan, Thermal performance of a phase change material-based heat sink in presence of nanoparticles and metal-foam to enhance cooling performance of electronics. *Journal of Energy Storage*, **2022**. 48: 103882.
[77] Matsumoto, K, D Shirai, Y Furudate, D Tsubaki, H Kubota, K Sekine, K Minamiya, Active control of supercooling degree using surfactant (In system with solid–liquid interface). *International Journal of Refrigeration*, **2015**. 58: 199-206.
[78] Guglielmero, L, A Mezzetta, L Guazzelli, C S Pomelli, F D'Andrea, C Chiappe, Systematic Synthesis and Properties Evaluation of Dicationic Ionic Liquids, and a Glance Into a Potential New Field. *Frontiers in Chemistry*, **2018**. 6: 612.
[79] Kenisarin, M, K Mahkamov, Solar energy storage using phase change materials. *Renewable and Sustainable Energy Reviews*, **2007**. 11(9): 1913-1965.
[80] Rebelo, L P N, J N C Lopes, J M S S Esperança, H J R Guedes, J Łachwa, V Najdanovic-Visak, Z P Visak, Accounting for the Unique, Doubly Dual Nature of Ionic Liquids from a Molecular Thermodynamic and Modeling Standpoint. *Accounts of Chemical Research*, **2007**. 40(11): 1114-1121.
[81] Yang, J, G-Q Qi, Y Liu, R-Y Bao, Z-Y Liu, W Yang, B-H Xie, M-B Yang, Hybrid graphene aerogels/phase change material composites: Thermal conductivity, shape-stabilization and light-to-thermal energy storage. *Carbon*, **2016**. 100: 693-702.
[82] Qiu, J, X Fan, Y Shi, S Zhang, X Jin, W Wang, B Tang, PEG/3D graphene oxide network form-stable phase change materials with ultrahigh filler content. *Journal of Materials Chemistry A*, **2019**. 7(37): 21371-21377.
[83] Deng, Q, H Wang, Z Xie, Y Tian, X Zhu, R Chen, Q Liao, Fast-freezing behavior of water droplet on subcooled superhydrophobic surface in DC electrostatic field. *International Journal of Thermal Sciences*, **2022**. 174: 107439.
[84] Shibata, M, S Sawayama, M Osugi, K Fujii, Structural aspect on "Salting-in" mechanism of PEG chains into a phosphonium-based ionic liquid using lithium salt. *Journal of Molecular Liquids*, **2022**. 366: 120255.
[85] Calado, M S, A S H Branco, V Najdanovic-Visak, Z P Visak, Solubility of high-value compounds in environmentally friendly solvents–liquid poly(ethylene glycol) and ionic liquids: Experimental study and thermodynamic analysis. *The Journal of Chemical Thermodynamics*, **2014**. 70: 154-159.
[86] Visak, Z P, M S Calado, J M Vuksanovic, G R Ivanis, A S H Branco, N D Grozdanic, M L Kijevcanin, S P Serbanovic, Solutions of ionic liquids with diverse aliphatic and aromatic solutes – Phase behavior

and potentials for applications: A review article. *Arabian Journal of Chemistry*, **2019**. 12(7): 1628-1640.
[87] Mahura, T, I Bahadur, P Naidoo, D Ramjugernath, Probing the ion-dipole interactions between the imidazolium-based ionic liquids and polyethylene glycol 200 using excess thermodynamic and spectroscopy studies. *Journal of Molecular Liquids*, **2022**. 350: 118519.
[88] Rodríguez, H, M Francisco, M Rahman, N Sun, R D Rogers, Biphasic liquid mixtures of ionic liquids and polyethylene glycols. *Physical Chemistry Chemical Physics*, **2009**. 11(46): 10916-10922.
[89] Mehrdad, A, N Noorani, Spectroscopic and density functional theory study on the interactions between 1-alkyl-3-methylimidazolium bromide ionic liquids with polyethylene glycol. *The Journal of Chemical Thermodynamics*, **2019**. 132: 38-43.
[90] Moosavi, M, A Daneshvar, Synergistic effects and specific molecular interactions in the binary mixtures of [bmim][BF4] and poly (ethylene glycol)s. *Journal of Molecular Liquids*, **2017**. 225: 810-821.
[91] Bosse, D, H-J Bart, Viscosity Calculations on the Basis of Eyring's Absolute Reaction Rate Theory and COSMOSPACE. *Industrial & Engineering Chemistry Research*, **2005**. 44(22): 8428-8435.
[92] Luo, Q, P Wei, Q Huang, B Gurkan, E B Pentzer, Carbon Capsules of Ionic Liquid for Enhanced Performance of Electrochemical Double-Layer Capacitors. *ACS Applied Materials & Interfaces*, **2018**. 10(19): 16707-16714.
[93] Gao, H, J Xing, X Xiong, Y Li, W Li, Q Liu, Y Wu, H Liu, Immobilization of Ionic Liquid [BMIM][PF6] by Spraying Suspension Dispersion Method. *Industrial & Engineering Chemistry Research*, **2008**. 47(13): 4414-4417.
[94] Li, H, Q Wang, H Wang, Y Cui, Y Zhu, B Wang, Fabrication of Thermally Stable Polysulfone Microcapsules Containing [EMIm][NTf2] Ionic Liquid for Enhancement of In Situ Self-Lubrication Effect of Epoxy. *Macromolecular Materials and Engineering*, **2016**. 301(12): 1473-1481.
[95] Weiss, E, B Dutta, A Kirschning, R Abu-Reziq, BMIm-PF6@SiO2 Microcapsules: Particulated Ionic Liquid as A New Material for the Heterogenization of Catalysts. *Chemistry of Materials*, **2014**. 26(16): 4781-4787.
[96] Palomar, J, J Lemus, N Alonso-Morales, J Bedia, M A Gilarranz, J J Rodriguez, Encapsulated ionic liquids (ENILs): from continuous to discrete liquid phase. *Chemical Communications*, **2012**. 48(80): 10046-10048.
[97] Luo, Q, Y Wang, Z Chen, P Wei, E Yoo, E Pentzer, Pickering Emulsion-Templated Encapsulation of Ionic Liquids for Contaminant Removal. *ACS Applied Materials & Interfaces*, **2019**. 11(9): 9612-9620.
[98] Yan, J, F Mangolini, Engineering encapsulated ionic liquids for next-generation applications. *RSC Advances*, **2021**. 11(57): 36273-36288.
[99] Weiss, E, D Gertopski, M K Gupta, R Abu-Reziq, Encapsulation of ionic liquid BMIm[PF6] within polyurea microspheres. *Reactive and Functional Polymers*, **2015**. 96: 32-38.
[100] Ma, Y, Z Li, H Wang, H Li, Synthesis and optimization of polyurethane microcapsules containing [BMIm]PF6 ionic liquid lubricant. *Journal of Colloid and Interface Science*, **2019**. 534: 469-479.
[101] Gaur, S S, K J Edgehouse, A Klemm, P Wei, B Gurkan, E B Pentzer, Capsules with polyurea shells and ionic liquid cores for CO2 capture. *Journal of Polymer Science*, **2021**. 59(23): 2980-2989.
[102] Lee, Y-Y, K Edgehouse, A Klemm, H Mao, E Pentzer, B Gurkan, Capsules of Reactive Ionic Liquids for Selective Capture of Carbon Dioxide at Low Concentrations. *ACS Applied Materials & Interfaces*, **2020**. 12(16): 19184-19193.

[103] Huang, Q, Q Luo, Y Wang, E Pentzer, B Gurkan, Hybrid Ionic Liquid Capsules for Rapid CO2 Capture. *Industrial & Engineering Chemistry Research*, **2019**. 58(24): 10503-10509.
[104] Weiss, E, R Abu-Reziq, Ionic liquid-based polymeric microreactors and their applicability. *Journal of Materials Science*, **2017**. 52(17): 10637-10647.
[105] Yang, M, X Zhu, G Ren, X Men, F Guo, P Li, Z Zhang, Tribological Behaviors of Polyurethane Composite Coatings Filled with Ionic Liquid Core/Silica Gel Shell Microcapsules. *Tribology Letters*, **2015**. 58(1): 9.
[106] Wang, P, J Zhu, J Tang, J Kang, L Shi, Morphology and CO2 adsorption performance of novel ionic liquid microcapsules containing [Bmim][PF6]. *Chemical Engineering Research and Design*, **2022**. 187: 633-644.
[107] Wang, H, J Zhu, L Tan, M Zhou, S Zhang, Encapsulated ionic liquids for CO2 capture. *Materials Chemistry and Physics*, **2020**. 251: 122982.
[108] Bernard, F L, E A Duarte, B B Polesso, R B Duczinski, S Einloft, CO2 sorption using encapsulated imidazolium-based fluorinated ionic liquids. *Environmental Challenges*, **2021**. 4: 100109.
[109] Nisar, M, F L Bernard, E Duarte, V V Chaban, S Einloft, New polysulfone microcapsules containing metal oxides and ([BMIM] [NTf2]) ionic liquid for CO2 capture. *Journal of Environmental Chemical Engineering*, **2021**. 9(1).
[110] Chen, D X, X K OuYang, Y G Wang, L Y Yang, K J Wu, C H He, Adsorption of caprolactam from aqueous solution by novel polysulfone microcapsules containing [Bmim][PF6]. *Colloids and Surfaces A: Physicochemical and Engineering Aspects*, **2014**. 441: 72-76.
[111]Bandeira, P, J Monteiro, A M Baptista, F D Magalhaes, Tribological Performance of PTFE-based Coating Modified with Microencapsulated [HMIM][NTf2] Ionic Liquid. *Tribology Letters*, **2015**. 59(1).
[112] Lak, S N, S Ahmed, P J Shamberger, E B Pentzer, Encapsulation of hygroscopic liquids via polymer precipitation in non-aqueous emulsions. *Journal of Colloid and Interface Science*, **2022**. 628: 605-613.
[113] Li, C M, Z Z Su, J J Tan, Y Xue, Y M Yang, H Y Yin, G X Zhang, Q Y Zhang, Autocatalyzed interfacial thiol-isocyanate click reactions for microencapsulation of ionic liquids. *Journal of Materials Science*, **2020**. 55(21): 9119-9128.
[114] Blokhin, A V, Y U Paulechka, G J Kabo, Formation of metastable crystals of [C4mim][NTf2] and [C6mim][NTf2]. *Thermochimica Acta*, **2006**. 445(1): 75-77.
[115] Das, T, T Lookman, M M Bandi, Morphology dictated heterogeneous dynamics in two-dimensional aggregates. *Soft Matter*, **2016**. 12(48): 9674-9682.
[116] Abe, H, H Kishimura, Multistep phase transition in 1-decyl-3-methylimidazolium nitrate ionic liquid. *Journal of Molecular Liquids*, **2022**. 352: 118695.
[117] Rotnicki, K, A Sterczyńska, Z Fojud, M Jażdżewska, A Beskrovnyi, J Waliszewski, M Śliwińska-Bartkowiak, Phase transitions, molecular dynamics and structural properties of 1-Ethyl-3-methylimidazolium bis(trifluoromethylsulfonyl)imide ionic liquid. *Journal of Molecular Liquids*, **2020**. 313: 113535.
[118] Weingärtner, H, Understanding ionic liquids at the molecular level: Facts, problems, and controversies. *Angewandte Chemie - International Edition*, **2008**. 47(4): 654-670.
[119] Zhang, S, J Wang, X Lu, Q Zhou, *Structures and Interactions of Ionic Liquids*. Structure and Bonding. Vol. 151. 2014: Springer Berlin, Heidelberg. VII, 197.
[120] Price, S L, From crystal structure prediction to polymorph prediction: Interpreting the crystal energy landscape. *Physical Chemistry Chemical Physics*, **2008**. 10(15): 1996-2009.

[121] Wang, L-M, V Velikov, C A Angell, Direct determination of kinetic fragility indices of glassforming liqu ids by differential scanning calorimetry: Kinetic versus thermodynamic fragilities. *The Journal of Chemical Physics*, **2002**. 117(22): 10184-10192.
[122] Stevenson, J D, P G Wolynes, Thermodynamic−Kinetic Correlations in Supercooled Liquids: A Critical Survey of Experimental Data and Predictions of the Random First-Order Transition Theory of Glasses. *The Journal of Physical Chemistry B*, **2005**. 109(31): 15093-15097.
[123] Shimizu, Y, Y Ohte, Y Yamamura, K Saito, T Atake, Low-Temperature Heat Capacity of Room-Temperature Ionic Liquid, 1-Hexyl-3-methylimidazolium Bis(trifluoromethylsulfonyl)imide. *The Journal of Physical Chemistry B*, **2006**. 110(28): 13970-13975.
[124] Paulechka, Y U, A V Blokhin, G J Kabo, A A Strechan, Thermodynamic properties and polymorphism of 1-alkyl-3-methylimidazolium bis(triflamides). *The Journal of Chemical Thermodynamics*, **2007**. 39(6): 866-877.
[125] Berthod, A, M J Ruiz-Ángel, S Carda-Broch, Recent advances on ionic liquid uses in separation techniques. *Journal of Chromatography A*, **2018**. 1559: 2-16.
[126] Keshavarz, M H, H R Pouretedal, E Saberi, A novel method for predicting melting point of ionic liquids. *Process Safety and Environmental Protection*, **2018**. 116: 333-339.
[127] Awad, W H, J W Gilman, M Nyden, R H Harris, T E Sutto, J Callahan, P C Trulove, H C DeLong, D M Fox, Thermal degradation studies of alkyl-imidazolium salts and their application in nanocomposites. *Thermochimica Acta*, **2004**. 409(1): 3-11.
[128] Zheng, J, Z Li, D Zhang, Q Yang, X Zhao, B Zhang, Y Wang, Thermal decomposition behavior, thermal stability and thermal explosion risk evaluation of a novel green hydroxylamine ionic liquid salt. *Journal of Molecular Liquids*, **2022**. 348: 118407.
[129] Ning Ren, F W, Jianjun Zhang,Xinfang Zheng, Progress in Thermal Analysis Kinetics. *Acta Physico-Chimica Sinica*, **2020**. 36(6): 1905062.
[130] Villanueva, M, A Coronas, J García, J Salgado, Thermal Stability of Ionic Liquids for Their Application as New Absorbents. *Industrial & Engineering Chemistry Research*, **2013**. 52(45): 15718-15727.
[131] Kosmulski, M, J Gustafsson, J B Rosenholm, Thermal stability of low temperature ionic liquids revisited. *Thermochimica Acta*, **2004**. 412(1): 47-53.
[132] Muhammad, A, M I Abdul Mutalib, C D Wilfred, T Murugesan, A Shafeeq, Thermophysical properties of 1-hexyl-3-methyl imidazolium based ionic liquids with tetrafluoroborate, hexafluorophosphate and bis(trifluoromethylsulfonyl)imide anions. *Journal of Chemical Thermodynamics*, **2008**. 40(9): 1433-1438.
[133] Del Sesto, R E, T M McCleskey, C Macomber, K C Ott, A T Koppisch, G A Baker, A K Burrell, Limited thermal stability of imidazolium and pyrrolidinium ionic liquids. *Thermochimica Acta*, **2009**. 491(1): 118-120.
[134] Rout, A, K Chandran, M Lavanya, N Ramanathan, Thermal stability assessment of a completely incinerable ionic liquid system in presence of nitric acid – A calorimetric study. *Thermochimica Acta*, **2021**. 700: 178939.
[135] Cao, Y, T Mu, Comprehensive Investigation on the Thermal Stability of 66 Ionic Liquids by Thermogravimetric Analysis. *Industrial & Engineering Chemistry Research*, **2014**. 53(20): 8651-8664.
[136] Tokuda, H, K Hayamizu, K Ishii, M A B H Susan, M Watanabe, Physicochemical Properties and Structures of Room Temperature Ionic Liquids. 2. Variation of Alkyl Chain Length in Imidazolium Cation. *The Journal of Physical Chemistry B*, **2005**. 109(13): 6103-6110.

[137] Smart, K, T D Golden, W E Acree, Investigations of potential ionic liquid phases for chromatographic processes using spectroscopic and thermal techniques. *Journal of Molecular Liquids*, **2022**. 363: 119820.
[138] Khajeh, A, M H Rahman, T Liu, P Panwar, P L Menezes, A Martini, Thermal decomposition of phosphonium salicylate and phosphonium benzoate ionic liquids. *Journal of Molecular Liquids*, **2022**. 352: 118700.
[139] Deferm, C, A Van den Bossche, J Luyten, H Oosterhof, J Fransaer, K Binnemans, Thermal stability of trihexyl(tetradecyl)phosphonium chloride. *Physical Chemistry Chemical Physics*, **2018**. 20(4): 2444-2456.
[140] Bender, C R, B L Kuhn, C A A Farias, F I Ziembowicz, T S Beck, C P Frizzo, Thermal stability and kinetic of decomposition of mono- And dicationic imidazolium-based ionic liquids. *Journal of the Brazilian Chemical Society*, **2019**. 30(10): 2199-2209.
[141] Gómez, E, N Calvar, Á Domínguez, E A Macedo, Thermal behavior and heat capacities of pyrrolidinium-based ionic liquids by DSC. *Fluid Phase Equilibria*, **2018**. 470: 51-59.
[142] Ge, R, C Hardacre, J Jacquemin, P Nancarrow, D W Rooney, Heat Capacities of Ionic Liquids as a Function of Temperature at 0.1 MPa. Measurement and Prediction. *Journal of Chemical & Engineering Data*, **2008**. 53(9): 2148-2153.
[143] Paulechka, Y U, A G Kabo, A V Blokhin, G J Kabo, M P Shevelyova, Heat Capacity of Ionic Liquids: Experimental Determination and Correlations with Molar Volume. *Journal of Chemical & Engineering Data*, **2010**. 55(8): 2719-2724.
[144] Bendová, M, Z Wagner, M G Bogdanov, M Čanji, N Zdolšek, Heat capacity of 1-hexadecyl-3-methylimidazolium based ionic liquids in solid and liquid phase. *Journal of Molecular Liquids*, **2020**. 305: 112847.
[145] Oster, K, P Goodrich, J Jacquemin, C Hardacre, A P C Ribeiro, A Elsinawi, A new insight into pure and water-saturated quaternary phosphonium-based carboxylate ionic liquids: Density, heat capacity, ionic conductivity, thermogravimetric analysis, thermal conductivity and viscosity. *The Journal of Chemical Thermodynamics*, **2018**. 121: 97-111.
[146] Carrete, J, T Méndez-Morales, M García, J Vila, Ó Cabeza, L J Gallego, L M Varela, Thermal Conductivity of Ionic Liquids: A Pseudolattice Approach. *The Journal of Physical Chemistry C*, **2012**. 116(1): 1265-1273.
[147] Murphy, T, L M Varela, G B Webber, G G Warr, R Atkin, Nanostructure–Thermal Conductivity Relationships in Protic Ionic Liquids. *The Journal of Physical Chemistry B*, **2014**. 118(41): 12017-12024.
[148] Nieto de Castro, C A, A P d C Ribeiro, A O Figueiras, E Langa, S I C Vieira, M J V Lourenço, Â F S d Santos, F J Vieira dos Santos, I M S Lampreia, P Goodrich, C Hardacre, Thermophysical Properties of 1-Butyl-3-methylimidazolium tris(pentafluoroethyl)trifluorophosphate, [C4mim][(C2F5)3PF3], and of Its IoNanofluid with Multi-Walled Carbon Nanotubes. *Journal of Chemical & Engineering Data*, **2021**. 66(4): 1717-1729.
[149] Mousavi, S P, S Atashrouz, F Rezaei, M-E Peyvastegan, A Hemmati-Sarapardeh, A Mohaddespour, Modeling thermal conductivity of ionic liquids: A comparison between chemical structure and thermodynamic properties-based models. *Journal of Molecular Liquids*, **2021**. 322: 114911.
[150] Phadungphatthanakoon, S, S Poompradub, S P Wanichwecharungruang, Increasing the Thermal Storage Capacity of a Phase Change Material by Encapsulation: Preparation and Application in Natural Rubber. *ACS Applied Materials & Interfaces*, **2011**. 3(9): 3691-3696.

[151] He, F, X Wang, D Wu, Phase-change characteristics and thermal performance of form-stable n-alkanes/silica composite phase change materials fabricated by sodium silicate precursor. *Renewable Energy*, **2015**. 74: 689-698.
[152] Zhang, H, X Wang, D Wu, Silica encapsulation of n-octadecane via sol–gel process: A novel microencapsulated phase-change material with enhanced thermal conductivity and performance. *Journal of Colloid and Interface Science*, **2010**. 343(1): 246-255.
[153] Liang, S, Q Li, Y Zhu, K Chen, C Tian, J Wang, R Bai, Nanoencapsulation of n-octadecane phase change material with silica shell through interfacial hydrolysis and polycondensation in miniemulsion. *Energy*, **2015**. 93: 1684-1692.
[154] Zhang, Y, Q Yue, M M Zagho, J Zhang, A A Elzatahry, Y Jiang, Y Deng, Core–Shell Magnetic Mesoporous Silica Microspheres with Large Mesopores for Enzyme Immobilization in Biocatalysis. *ACS Applied Materials & Interfaces*, **2019**. 11(10): 10356-10363.
[155] Song, W, M Song, W Cai, W Li, X Jiang, W Fang, W Lai, Efficient and stable SiO2-encapsulated NiPt/HY catalyst for catalytic cracking of β-O-4 linkage compound. *Renewable Energy*, **2022**. 198: 334-342.
[156] Kang, L, L Ren, H Niu, R Lv, H Guo, S Bai, Paraffin@SiO2 microcapsules-based phase change composites with enhanced thermal conductivity for passive battery cooling. *Composites Science and Technology*, **2022**. 230: 109756.
[157] Li, Y, Q Liu, Y Liu, D Wang, W Song, Y Chen, J Liu, Calcium chloride hexahydrate/nano-SiO2 composites as form-stable phase change materials for building energy conversation: The influence of pore size of nano-SiO2. *Energy and Buildings*, **2020**. 208: 109672.
[158] Sun, X, M Yi, B Feng, R Liu, L Sun, L Zhai, H Cao, C Zou, Shape-stabilized composite phase change material PEG@TiO2 through in situ encapsulation of PEG into 3D nanoporous TiO2 for thermal energy storage. *Renewable Energy*, **2021**. 170: 27-37.
[159] Li, B, D Shu, R Wang, L Zhai, Y Chai, Y Lan, H Cao, C Zou, Polyethylene glycol/silica (PEG@SiO2) composite inspired by the synthesis of mesoporous materials as shape-stabilized phase change material for energy storage. *Renewable Energy*, **2020**. 145: 84-92.
[160] Chen, S, G Wu, M Sha, S Huang, Transition of Ionic Liquid [bmim][PF6] from Liquid to High-Melting-Point Crystal When Confined in Multiwalled Carbon Nanotubes. *Journal of the American Chemical Society*, **2007**. 129(9): 2416-2417.
[161] Zeeshan, M, V Nozari, M B Yagci, T Isık, U Unal, V Ortalan, S Keskin, A Uzun, Core–Shell Type Ionic Liquid/Metal Organic Framework Composite: An Exceptionally High CO2/CH4 Selectivity. *Journal of the American Chemical Society*, **2018**. 140(32): 10113-10116.
[162] Denny, M S, J C Moreton, L Benz, S M Cohen, Metal–organic frameworks for membrane-based separations. *Nature Reviews Materials*, **2016**. 1(12): 16078.
[163] Duan, J, W Jin, S Kitagawa, Water-resistant porous coordination polymers for gas separation. *Coordination Chemistry Reviews*, **2017**. 332: 48-74.
[164] Yi, S-M, C-R Zhang, W Jiang, X Liu, C-P Niu, J-X Qi, X-J Chen, R-P Liang, J-D Qiu, Ionic liquid modified covalent organic frameworks for efficient detection and adsorption of ReO4–/TcO4–. *Journal of Environmental Chemical Engineering*, **2022**. 10(3): 107666.
[165] Liu, X, F Yang, L Wu, Q Zhou, R Ren, Y k Lv, Ionic liquid-loaded covalent organic frameworks with favorable electrochemical properties as a potential electrode material. *Microporous and Mesoporous Materials*, **2022**. 336: 111906.
[166] Gulbalkan, H C, Z P Haslak, C Altintas, A Uzun, S Keskin, Assessing CH4/N2 separation

potential of MOFs, COFs, IL/MOF, MOF/Polymer, and COF/Polymer composites. *Chemical Engineering Journal*, **2022**. 428: 131239.
[167] Pandey, D K, D Jadav, T Patil, S Dharaskar, N Tsunoji, R Kumar, D K Singh, M Bandyopadhyay, Ordered mesoporous silica matrices supported ionic liquids for efficient CO2 separation from CO2/CH4 gas mixture: Experimental and theoretical investigation. *Journal of Molecular Liquids*, **2022**. 368: 120569.
[168] Qin, J, Y Wang, Z Gan, W Ma, F Huo, Y Nie, C Yang, H He, Manipulating mechanism of the electrokinetic flow of ionic liquids confined in silica nanochannel. *Chemical Engineering Science*, **2022**. 260: 117913.
[169] Bai, J, B Zhang, B Yang, J Shang, Z Wu, Preparation of three-dimensional interconnected graphene/ionic liquid composites to enhanced thermal conductivities for battery thermal management. *Journal of Cleaner Production*, **2022**. 370: 133572.
[170] Cai, J, L Lu, J Zhu, Z Weng, Ionic-liquid-gated porous graphene membranes for efficient CO2/CH4 separation. *Journal of Molecular Liquids*, **2022**. 358: 119148.
[171] Pietrzak, K, C Wardak, Comparative study of nitrate all solid state ion-selective electrode based on multiwalled carbon nanotubes-ionic liquid nanocomposite. *Sensors and Actuators B: Chemical*, **2021**. 348: 130720.
[172] Boldoo, T, V Chinnasamy, M Kim, H Cho, CO2 entrapment using 1–hexyl- 3–methyl-imidazolium room temperature ionic liquids with multi-walled carbon nanotubes. *Journal of CO2 Utilization*, **2022**. 66: 102285.
[173] Huang, Z, S Liu, Q Geng, H Zeng, Y Li, S Xu, S M Sadeghzadeh, Sustainable production of biodiesel using nanocluster giant lemon nanopolyoxomolybdate supported on carbon nanotubes by ionic liquid. *Inorganic Chemistry Communications*, **2022**. 142: 109714.
[174] Li, X, O J Curnow, J Choi, A C K Yip, Recent advances in the imidazolium-based ionic liquid-templated synthesis of microporous zeolites. *Materials Today Chemistry*, **2022**. 26: 101133.
[175] Abu Zarin, M A, M M Zainol, N A S Ramli, N A S Amin, Zeolite immobilized ionic liquid as an effective catalyst for conversion of biomass derivatives to levulinic acid. *Molecular Catalysis*, **2022**. 528: 112506.
[176] Comin, E, A S Aquino, C Favero, M L Mignoni, R F de Souza, M O de Souza, S B C Pergher, C X d S Campos, K Bernardo-Gusmão, Cyclic carbonate synthesis via cycloaddition of CO2 and epoxides catalysed by beta zeolites containing alkyl imidazolium ionic liquids used as structure-directing agents. *Molecular Catalysis*, **2022**. 530: 112624.
[177] Chen, S, Y Liu, H Fu, Y He, C Li, W Huang, Z Jiang, G Wu, Unravelling the Role of the Compressed Gas on Melting Point of Liquid Confined in Nanospace. *The Journal of Physical Chemistry Letters*, **2012**. 3(8): 1052-1055.
[178] Zhang, S, J Zhang, Y Zhang, Y Deng, Nanoconfined Ionic Liquids. *Chemical Reviews*, **2017**. 117(10): 6755-6833.
[179] Wu, C-M, S-Y Lin, K-Y Kao, H-L Chen, Self-Organization of a Hydrophilic Short-Chain Ionic Liquid Confined within a Hydrophobic Nanopore. *The Journal of Physical Chemistry C*, **2014**. 118(31): 17764-17772.
[180] Wu, C-M, S-Y Lin, Close Packing Existence of Short-Chain Ionic Liquid Confined in the Nanopore of Silica Ionogel. *The Journal of Physical Chemistry C*, **2015**. 119(22): 12335-12344.
[181] Iacob, C, J R Sangoro, W K Kipnusu, R Valiullin, J Kärger, F Kremer, Enhanced charge transport in nano-confined ionic liquids. *Soft Matter*, **2012**. 8(2): 289-293.

[182] Li, S, K S Han, G Feng, E W Hagaman, L Vlcek, P T Cummings, Dynamic and Structural Properties of Room-Temperature Ionic Liquids near Silica and Carbon Surfaces. *Langmuir*, **2013**. 29(31): 9744-9749.
[183] Han, K S, X Wang, S Dai, E W Hagaman, Distribution of 1-Butyl-3-methylimidazolium Bistrifluoromethylsulfonimide in Mesoporous Silica As a Function of Pore Filling. *The Journal of Physical Chemistry C*, **2013**. 117(30): 15754-15762.
[184] Martinelli, A, M Maréchal, Å Östlund, J Cambedouzou, Insights into the interplay between molecular structure and diffusional motion in 1-alkyl-3-methylimidazolium ionic liquids: a combined PFG NMR and X-ray scattering study. *Physical Chemistry Chemical Physics*, **2013**. 15(15): 5510-5517.
[185] Néouze, M-A, J Le Bideau, P Gaveau, S Bellayer, A Vioux, Ionogels, New Materials Arising from the Confinement of Ionic Liquids within Silica-Derived Networks. *Chemistry of Materials*, **2006**. 18(17): 3931-3936.
[186] Wang, Y, C Li, X Guo, G Wu, The Influence of Silica Nanoparticles on Ionic Liquid Behavior: A Clear Difference between Adsorption and Confinement. *International Journal of Molecular Sciences*, **2013**. 14(10): 21045-21052.
[187] Verma, Y L, R K Singh, Conformational States of Ionic Liquid 1-Ethyl-3-methylimidazolium Bis(trifluoromethylsulfonyl)imide in Bulk and Confined Silica Nanopores Probed by Crystallization Kinetics Study. *The Journal of Physical Chemistry C*, **2015**. 119(43): 24381-24392.
[188] Gupta, A K, R K Singh, S Chandra, Crystallization kinetics behavior of ionic liquid [EMIM][BF4] confined in mesoporous silica matrices. *RSC Advances*, **2014**. 4(42): 22277-22287.
[189] Naffakh, M, C Marco, M A Gómez-Fatou, Isothermal crystallization kinetics of novel isotactic polypropylene/MoS2 inorganic nanotube nanocomposites. *Journal of Physical Chemistry B*, **2011**. 115(10): 2248-55.
[190] Zhou, R-B, H-L Cao, C-Y Zhang, D-C Yin, A review on recent advances for nucleants and nucleation in protein crystallization. *CrystEngComm*, **2017**. 19(8): 1143-1155.
[191] Zheng, L, J Li, M Yu, W Jia, S Duan, D Cao, X Ding, B Yu, X Zhang, F-J Xu, Molecular Sizes and Antibacterial Performance Relationships of Flexible Ionic Liquid Derivatives. *Journal of the American Chemical Society*, **2020**. 142(47): 20257-20269.
[192] Mu, C, J Pang, Q Lu, T Liu, Effects of surface topography of material on nucleation site density of dropwise condensation. *Chemical Engineering Science*, **2008**. 63(4): 874-880.
[193] Zeng, Q, A simple method for estimating the size of nuclei on fractal surfaces. *Journal of Crystal Growth*, **2017**. 475: 49-54.
[194] Stolyarova, S, E Baskin, Y Nemirovsky, Enhanced crystallization on porous silicon: Facts and models. *Journal of Crystal Growth*, **2012**. 360: 131-133.
[195] Zeng, Q, K Li, T Fen-Chong, Heterogeneous nucleation of ice from supercooled NaCl solution confined in porous cement paste. *Journal of Crystal Growth*, **2015**. 409: 1-9.
[196] Sun, Y, H Chang, J Hu, Y Wang, Y Weng, C Zhang, S Niu, L Cao, Z Chen, N Guo, J Liu, J Chi, G Li, L Xiao, Large-Scale Multifunctional Carbon Nanotube Thin Film as Effective Mid-Infrared Radiation Modulator with Long-Term Stability. *Advanced Optical Materials*, **2021**. 9(3): 2001216.
[197] Zhao, L, R Zhang, C Deng, Y Peng, T Jiang, Tunable Infrared Emissivity in Multilayer Graphene by Ionic Liquid Intercalation. *Nanomaterials*, **2019**. 9(8): 1096.
[198] Ergoktas, M S, G Bakan, P Steiner, C Bartlam, Y Malevich, E Ozden-Yenigun, G He, N Karim, P Cataldi, M A Bissett, I A Kinloch, K S Novoselov, C Kocabas, Graphene-Enabled Adaptive Infrared Textiles. *Nano Letters*, **2020**. 20(7): 5346-5352.

[199] Chen, J, S Zhang, Y Wei, J Yi, W Pang, H Zhang, Y Fu, C Li, W Xia, C Xiong, Flexible human-applicable infrared camouflage materials with temperature and emissivity tunability. *Composites Science and Technology*, **2023**. 233: 109920.
[200] Hu, J, Y Hu, Y Ye, R Shen, Unique applications of carbon materials in infrared stealth: A review. *Chemical Engineering Journal*, **2023**. 452: 139147.
[201] Tang, X, T Xu, J Wang, H Zhang, J Chen, G Huang, Y Sun, D Wang, Y Liu, J Li, Preparation and thermal properties of a novel pseudo ionic liquid phase change material for solar water heating system. *Solar Energy Materials and Solar Cells*, **2022**. 236: 111507.
[202] Liu, J, Z Ye, L Zhang, X Fang, Z Zhang, A combined numerical and experimental study on graphene/ionic liquid nanofluid based direct absorption solar collector. *Solar Energy Materials and Solar Cells*, **2015**. 136: 177-186.
[203] Chereches̨, E I, D Bejan, C Ibanescu, M Danu, A A Minea, Ionanofluids with [C_2mim][CH_3SO_3] ionic liquid and alumina nanoparticles: An experimental study on viscosity, specific heat and electrical conductivity. *Chemical Engineering Science*, **2021**. 229: 116140.
[204] Mehrkesh, A, A T Karunanithi, Optimal design of ionic liquids for thermal energy storage. *Computers & Chemical Engineering*, **2016**. 93: 402-412.
[205] *Modified Ionic Liquid-Based Phase Change Materials as Effective Heat Exchangers, Phase I.* 2016 2022-09-16]; Available from: https://techport.nasa.gov/view/90050.
[206] Ben Romdhane, S, A Amamou, R Ben Khalifa, N M Saïd, Z Younsi, A Jemni, A review on thermal energy storage using phase change materials in passive building applications. *Journal of Building Engineering*, **2020**. 32: 101563.
[207] Ruiz, E, V R Ferro, J de Riva, D Moreno, J Palomar, Evaluation of ionic liquids as absorbents for ammonia absorption refrigeration cycles using COSMO-based process simulations. *Applied Energy*, **2014**. 123: 281-291.
[208] Wu, W, Low-temperature compression-assisted absorption thermal energy storage using ionic liquids. *Energy and Built Environment*, **2020**. 1(2): 139-148.
[209] Schultz, J M, S Furbo, Solar heating systems with heat of fusion storage with 100% solar fraction for solar low energy buildings. *In Proceedings of the International Solar Energy Society (ISES) World Congress 2007*, **2009**. 1-5: 2721− 2725.
[210] Bai, L, X Li, J Zhu, B Chen, Effects of Nucleators on the Thermodynamic Properties of Seasonal Energy Storage Materials Based on Ionic Liquids. *Energy & Fuels*, **2011**. 25(4): 1811-1816.